VNIVERSITAT DE VALÈNCIA

Doctorado en Nanociencia y Nanotecnología

Ph.D. Thesis:

Single junction and tandem perovskite solar cells

Ph.D. candidate:

Dávid Forgács

Supervisors:

Dr. Hendrik Jan Bolink

Dr. Michele Sessolo

Tutor:

Dr. Hendrik Jan Bolink

Septiembre 2017

Dr. Hendrik Jan Bolink y **Dr. Michele Sessolo**, Investigadores de la Universidad de Valencia en el Instituto de Ciencia Molecular (ICMol), certifican que la memoria presentada por el doctorando Dávid Forgács con el título "Single junction and tandem perovskite solar cells" corresponde a su Tesis Doctoral y ha sido realizada bajo su dirección y tutoría, autorizando mediante este escrito la presentación de la misma.

En Valencia, a 28 de Septiembre de 2017

Dr. Hendrik Jan Bolink
(director y tutor)

Dr. Michele Sessolo
(director)

"I arise in the morning torn between a desire to improve the world and a desire to enjoy the world. This makes it hard to plan the day."

- E.B. White

Table of Contents

Acknowledgements 9

1 Introduction 11

1.1 The emergence of perovskite solar cells 11

1.2 Perovskite basics – structure and properties 13

1.3 Thin film deposition methods 17

1.4 Solvent engineering 18

1.5 Precursor compositions 19

1.6 Device architectures 21

1.7 Band gap engineering 23

1.8 Tandem solar cells 26

2 Aim of the thesis 30

3 Experimental Methods 31

3.1 Substrate preparation 31

3.2 Solution processing of p-i-n solar cells 31

3.3 Solution processing of n-i-p solar cells 32

3.4 Evaporation of doped hole transport layers 32

3.5 Evaporation of metal electrodes 32

3.6 Solar cell characterization 33

3.7 UV-Vis spectrometry 33

3.8 Photoluminescence (PL) measurements 34

3.9 XRD measurements 34

3.10 AFM measurements 34

3.11 SEM measurements 35

4 Lead acetate based perovskite solar cells 36

5 Wide bandgap perovskite solar cells 43

6 Perovskite-perovskite tandem cells 50

7 Summary and outlook 58

8 Resumen en español 60

8.1 Introducción 60

8.1.1 El comienzo de las células solares de perovskita 60

8.1.2 Generalidades de las perovskitas: Estructura y propiedades 62

8.1.3 Métodos de deposición de películas delgadas 65

8.1.4 Ingeniería de disolventes 66
8.1.5 Composición de los precursores 67
8.1.6 Arquitectura de los dispositivos 69
8.1.7 Ingeniería de "bandgap" 70
8.1.8 Células solares tándem 72
8.2 Objetivo de la tesis 73
8.3 Células solares de perovskita basadas en acetato de plomo 74
8.4 Células solares de perovskita con elevado "bandgap" 75
8.5 Células tándem perovskita-perovskita 77
8.6 Resumen y perspectivas 78
Other contributions of the author 81
Bibliography 82

Acknowledgements

First of all, I would like to sincerely thank to my supervisor, Dr. Hendrik Jan Bolink, for accepting me into the group and providing me with his trust and care. His constant support and the freedom he provided me with made my Ph.D. experience wonderful and unforgettable. I am grateful for both his scientific and personal contribution to my well-being during the years I have spent in Valencia. My gratitude to Dr. Michele Sessolo as well, for his time and efforts in making the output of my scientific research sound much more amazing, and for the proofreading of my thesis. The coffee-scented discussions we shared were shedding light on the perovskite solar cells, and their future. I would like to thank Dr. Maria Monrabal Capilla for her ceaseless help and guidance through the labyrinths of bureaucracy. As much as our interactions did not start completely smooth, I am honored to call her a friend. Many thanks to Ángel López, for his altruistic help to overcome any technical problem, and especially for translating my thesis to Spanish. I would like to thank all my colleague-friends from ICMol for both their scientific input, and the amazing time we have spent together. It was a wonderful period, and I am sure our paths will cross in the future. I would like to thank Dr. Uli Würfel, Dr. Markus Kohlstädt and Dr. Martin Sessler, for teaching me the basics of organic semiconductors, tandem cells and their processing during the research of my Master Thesis. The knowledge proved invaluable during my Ph.D. research. Many thanks to Ralph Pätzold, Alexander Krönke and Bas Van der Wiel for welcoming me at Belectric OPV during my internship.

I would like to thank my Mom for her constant struggles against the odds to support me getting this far. I am thankful to all my friends spread around the world for being there for me. Lastly, I would like to thank to the staff of Radio City for regularly providing me the fuel for my creativity. ☺

1 Introduction

1.1 The emergence of perovskite solar cells

One of the major issues humankind has to solve during the 21st century is to meet the ever increasing energy demand, and to do so in a sustainable way. Harnessing renewable energy sources is a straightforward path to achieve it, and a global research effort is devoted to maximize the electrical power output from the most abundant ones. Solar energy is one of the most promising candidates, as there is a vast power reaching the Earth in the form of radiation from the sun. Albeit it is intermittent and unevenly distributed, it is the renewable energy source with the highest power density and hence the most promising alternative to replace carbon and nuclear based energy sources. The market for solar energy is steadily growing, and the 235 GW of total power provided by worldwide installations by the end of the year 2015 is expected to double by the end of 2018.[1] Photovoltaic (PV) devices provide direct transformation of solar energy to electricity, eliminating intermediate conversion steps used in most conventional energy production types. Since the announcement of the first rational silicon solar by Bell labs in 1954 with a power conversion efficiency (PCE) of 6%, modules based on this material have managed to reach commercial availability in a few years, dominating the PV market ever since.[2] The price of this source of electricity is steadily decreasing, and in many areas around the world it has already reached grid parity. While silica is an abundant and non-toxic material, its processing into a high purity crystalline silicon is an energy consuming and slow process. Also, being a semiconductor with an indirect band gap, its absorption coefficient is quite low, and as such a layer thickness of several microns is needed to achieve high efficiency solar cells.[3] These intrinsic shortcomings of crystalline silicon foster the development of cheaper and more efficient PV devices, based on alternative materials and preparation methods. Thin film solar cells, - usually referred to as the second generation of photovoltaics - utilize semiconducting materials that are orders of magnitude more efficient light absorbers compared to silicon,

enabling the manufacturing of devices with thinner photoactive layers, hence with less material consumption and possibly a cheaper energy production. The most important technologies are cadmium telluride (CdTe), copper indium gallium diselenide (CIGS), and hydrogenated amorphous silicon (a-Si:H).[4] While these approaches have already demonstrated their feasibility of commercialization, the corresponding market share remains below 10%. The third generation of solar cells consists of the emerging thin film PV technologies. This category utilizes advanced materials with special properties. These properties for instance can be the feasibility to utilize solution processing for the preparation of thin films or tandem architectures to surpass the Shockley-Quessier limit for single cells.[5] A promising candidate has been the dye-sensitized solar cell (DSSC) introduced by researchers at EPFL.[6] The prototype of such devices used mesoporous titanium dioxide (TiO_2) sensitized with dye molecules able to absorb light and transfer electrons to the TiO_2. The archetypical DSSCs suffer from two main drawbacks, i) the dye molecules contain rare metals such as ruthenium, making them less viable as a source of cheap energy, ii) they used a liquid electrolyte, detrimental for the solar cell lifetime. Both of these issues have been partially alleviated throughout the years, by developing metal-free dyes and solid-state electrolytes.[7] Nevertheless, DSSCs have been recently abandoned in favor of more efficient devices based on organic-inorganic (hybrid) halide perovskites as the light harvester, due to the exquisite properties of this group of materials described in the next section.

1.2 Perovskite basics – structure and properties

The general structure of three dimensional (3D) halide perovskites is ABX_3, where A and B are mono and divalent cations respectively, and X is an anion. The most common A-site cations are methylammonium (MA^+), formamidinium (FA^+) or cesium (Cs^+), however the incorporation of other cations, such as rubidium (Rb^+) or guanidinium (GA^+) has also been reported.[8,9] The B-site cations are typically lead (Pb^{2+}) or tin (Sn^{2+}), while the halides in photovoltaic applications are iodide (I^-) or bromide (Br^-). The ABX_3 formula was first described by Goldschmidt, who defined the perovskite tolerance factor, a dimensionless number that can be used to determine the lattice stability based on the size of the composing ions.[10] In general, stable 3D perovskites are predicted if the tolerance factor is between 0.8 and 1.[11] The tolerance factor is an important tool in theoretical calculations, as one can predict whether a composition of certain ions will be compatible with the perovskite structure, and thus it is used to guide experimental research in the development of new formulations for optoelectronic devices with high performance.

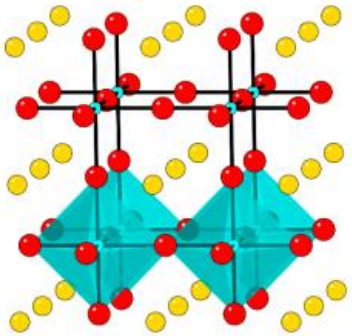

$$t = \frac{R_A + R_X}{\sqrt{2(R_B + R_X)}}$$

Fig. 1: A cubic perovskite structure of ABX_3, where A is yellow, B is cyan and X is red. On the right, the equation for the calculation of the Goldschmidt tolerance factor, where R_A R_B and R_X are the ionic radii of the A, B and X ions respectively.

The lattice parameter of the crystal structure depends on the effective anionic radius of the halides, which in turn determines the band gap of the semiconducting material. This has already been showed as early as 1978 by Weber, who obtained methylammonium lead halide perovskites of different colors ranging from colorless to black via varying the halide composition.[12] It means that the absorption onset of these materials can be tuned over the whole visible spectrum by a simple halide exchange. These properties are key features making perovskites extremely versatile materials, and it has been extensively investigated with the aim of tuning the band-gap of the photoactive layers in perovskite solar cells.[13] There are a number of interesting electronic properties that can arise due to the specific crystal structure of this group of materials. These include ferroelectricity, superconductivity, and even photovoltaic behavior.[14–16] Since the observation of photocurrents in barium titanate ($BaTiO_3$) in 1956, researchers tried to fabricate solar cells based on inorganic oxide perovskites, however their power conversion efficiency (PCE) remained below 1%. Mitzi et al. reported the simple and low temperature preparation of the organic-inorganic hybrid halide $CH_3NH_3SnI_3$ perovskite, and investigated its properties in 1995.[17] It was in 2009 when Miyasaka and coworkers used methylammonium lead bromide and iodide (MAPBr, MAPI) nanocrystals as sensitizers for DSSCs. They observed that the solar cells with MAPI absorbers showed a spectral sensitivity up to 800 nm, and obtained a PCE of 3.8%.[18] The devices prepared in this seminal work used the conventional liquid electrolyte used in the DSSCs, and hence led to a rapid degradation of the perovskite (soluble in polar solvents) and to the low efficiency of the solar cells. A major breakthrough came a few years later when the liquid electrolyte was replaced by a solid state organic semiconductor. In 2012, two reports demonstrated a large increase of the PV efficiency by using spiro-OMeTAD as the hole transport material (HTM). Kim et al. reported a solid state mesoscopic device based on MAPI nanoparticles (NPs), reaching a PCE of 9.7%.[19] Lee et al.

prepared a meso-superstructured perovskite solar cell with a polycrystalline MAPI absorber layer, achieving a PCE of 10.9%.[20] The latter work also investigated the effect of using an insulating Al_2O_3 scaffold instead of the traditional TiO_2. The fact that the solar cells prepared with the latter architecture were capable of delivering an even better performance compared to those using TiO_2 implied that the perovskite material was capable of ambipolar charge transport – transporting both electrons and holes to their respective electrodes.

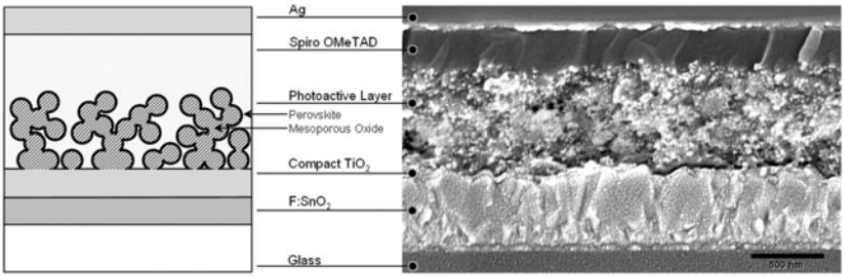

Fig. 2: The layout and cross-sectional SEM image of one of the first solid-state perovskite solar cells.

Hybrid perovskites have a range of other intrinsic and attractive properties which make them an excellent candidate for PV applications. De Wolf et al. investigated the optical absorption edge of organometallic halide perovskites, and its correlation to the photovoltaic performance.[21] They have used photothermal deflection spectroscopy (PDS) and Fourier-transform photocurrent spectroscopy (FTPS), both allowing a sensitive method for the measurement of absorption. They have found that these type of materials possess a steep absorption onset, which is comparable with GaAs, the best performing photovoltaic material to date. They have also measured an Urbach energy as small as 15 meV, which indicates a high degree of order in the material at the microscale. Their findings explained the low offset between the optical band gap of MAPI and the open circuit voltage (V_{oc}) of the corresponding solar cells, which is one of the

reasons for the high performance of such devices. Yin et al. performed a systematical theoretical study to investigate the unique properties of halide perovskites.[22] Their calculations confirmed an exceptionally high optical absorption coefficient, between 10^4 and 10^5 cm^{-1} in the visible part of the electromagnetic spectrum, values comparable with that of gallium arsenide (GaAs). The nature of the photogenerated charge carriers is of special importance, as it has implications on charge separation, transport and on the photovoltaic performance in general. The exciton binding energy is reported to be between 2 and 45 meV, in any case comparable to the thermal energy of 26 meV at room temperature.[23–25] Manser et al. investigated the charge carrier generation in perovskite films using femtosecond transient absorption spectroscopy.[26] They showed how after photoexcitation there is a significant interaction between excitons and free carriers, and that screening by the latter limits exciton formation. The presensce of mainly free carriers implies that a donor-acceptor interface is not required for the efficient operation of perovskite solar cells, and even the use of planar structures is a viable approach to reach high performance devices. Initially thought of as a sensitizer in DSSCs, perovskites were soon recognized as new thin-film absorbers, and these pioneering works initiated an extensive research on hybrid halide perovskites, now a stand-alone PV technology. In the following years, various methods were explored to deposit high quality perovskite materials. The focus was to understand how the chemistry of diverse precursors is affected by a multitude of processing techniques and conditions, and how it influences the optoelectronic properties of the deposited perovskite thin film. Establishing better control over these parameters allowed the preparation of devices with near to optimal performances. These efforts eventually led to solar cell efficiencies competing with record Si based ones in only a few years – with the current certified PCE record of 22.1% – consolidating perovskite photovoltaics as a potential alternative renewable energy source.[27] In the following we will review the main strategies explored so far to fabricate perovskite solar cells.

1.3 Thin film deposition methods

There are two major routes to deposit perovskite thin films, solution- and vacuum-based, depending on the medium used to carry the precursors onto the substrate. They can be further categorized based on the number of deposition steps used to form the perovskites, and in most cases films are formed through a one-step or a two-step method. The simplest and most straightforward approach is the one-step solution processing. In this case, the precursors (halide salts of the metal B and of the cation A) are dissolved in a polar solvent. Dimethylformamide (DMF) or dimethyl sulfoxide (DMSO) are the most widely used solvents, however alternatives such as γ-butyrolactone (GBL) or N-methyl-2-pyrrolidone (NMP) have also been investigated.[28] While the implementation of this approach is easy, gaining control over the morphology of the resulting film requires profound understanding of the complex processes involved in the perovskite formation. In two-step processing, the lead compound is deposited first, and afterwards it is converted to perovskite by reaction with the organic salt by spin- or dip coating. The advantage of this method is that it is simpler to control the deposition of the single compounds, and it allows the formation of homogeneous and continuous films. The major drawback of this method is that the final perovskite thickness is limited to a few hundred nanometers, due to the short diffusion depth of the organic compounds into the polycrystalline lead halide. This intrinsically limits the maximum achievable photocurrent and hence the maximum efficiency of the solar cell. Yang et al. developed the vapor assisted solution processing (VASP), a two-step method where the conversion is achieved by exposure of the lead halide to methylammonium iodide (MAI) vapors.[29] In fully vapor based methods, the precursors are placed into separate crucibles in a vacuum chamber, and then heated to their sublimation temperature. In this way their vapors condensed and react on the substrates forming compact perovskite films at low temperature.[30]

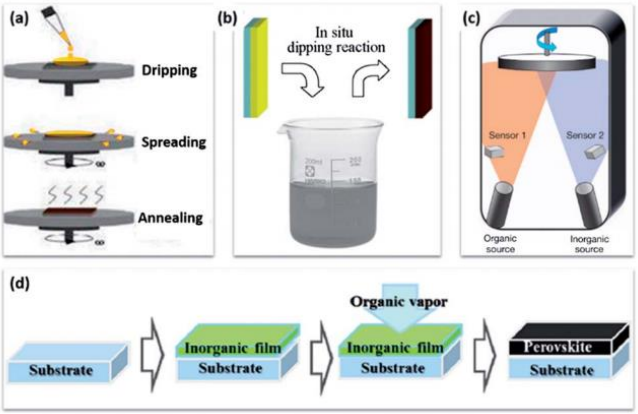

Fig. 3: The most common methods to deposit perovskite layers. A) one-step spin coating B) two-step method with dip coating C) coevaporation D) vapor assisted solution processing

A two-step method was adapted also to vacuum based processing.[31] Though the vacuum based processes are reliable, the vast majority of the published works utilized solution processing due to the simpler instrumentation and processing required. Thus the focus will be mainly on solution based approaches in the following.

1.4 Solvent engineering

As the nucleation and growth of the perovskite film strongly depends on the interactions of the solvent with the precursors and the substrate, it is important to choose an appropriate solvent and tune the deposition conditions. As such, the engineering of these parameters became an important part of the solution processed perovskite solar cell field. Initially solvent mixtures were explored to improve the morphology of the film. Later, Jeon et al. reported a method in which they used a mixture of GBL and DMSO for the precursor solution, and they treated the sample with toluene during spinning.[32] Toluene is miscible with both GBL and DMSO,

however it is a poor solvent for the perovskite precursors. If the wet film is treated with the anti-solvent in the proper time window, the residual solvents will be washed out immediately, and a uniform perovskite layer with large grain sizes will be left on the substrate. This approach has become widespread to deposit uniform layers that yield high performance devices, and the most efficient solar cells to date are fabricated with an anti-solvent strategy.[33,34]

1.5 Precursor compositions

Initial works used 1:1 stoichiometric mixtures of MAI and PbI_2, however it was observed that the morphology of the perovskite layers deposited from such precursors is poor. Rod-like structures were reported in several works, which does not lead to complete coverage of the substrate. The holes present in such films lower the shunt resistance of the corresponding solar cells, leading in many cases to current shunting and poor and unreliable performance. Several works addressed this problem, and by help of additives such as methylammonium chloride (MACl), 1,8-diodooctane (DIO), or hydroiodic acid (HI) in the precursor, a significant improvement in the film morphology was observed.[35,36] The works of Kim and Lee demonstrated that using $PbCl_2$ as the lead source results in improved device performance, mainly through more homogeneous morphology of the photoactive layer. The material was referred to as a "mixed halide perovskite", which they denoted as $CH_3NH_3PbI_2Cl$. Later, Colella et al. have shown that the mixed halide route in fact does not lead to a stoichiometric mixture of chloride and iodide, and chloride only remains as a trace in the material.[37] These findings initiated extensive research on the effect of precursor components and ratios on the performance of the resulting perovskite. The role of the precursor materials and anions were investigated by Moore et al., who concluded that the kinetics of the crystallization can be altered by choosing different lead precursors.[38]

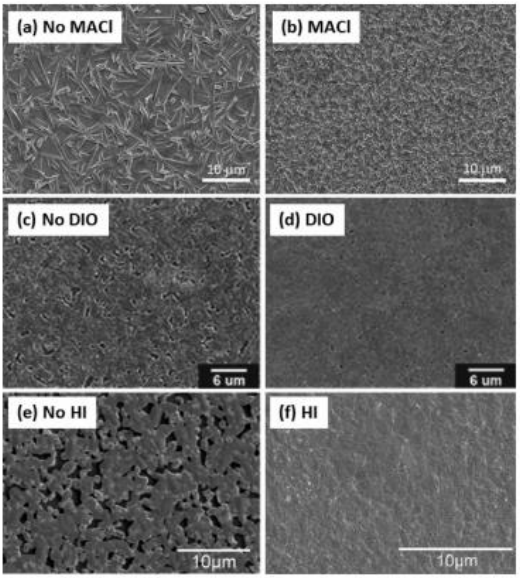

Fig. 4: Improving the morphology of perovskite thin films with various additives.

It was shown that if volatile materials can be formed, they can play a spectating role during crystallization, leaving the system during heat treatment and forming a pure and homogeneous perovskite film. These findings elucidated the role of chloride ions in the precursors and opened up possibilities for an augmented nucleation and growth at lower temperatures by using alternative precursors, such as $PbNO_3$ or lead acetate, $Pb(OAc)_2$. It has been observed that besides the composition of the precursor, the stoichiometric ratio of the components also has a large impact on the morphology of the deposited perovskite film and its photovoltaic performance. Yan et al. have performed a thorough analysis of different precursors, varying the ratio between the organic- and the lead halide.[39] The study has revealed that the perovskite precursor solutions are in fact colloidal dispersions, whose chemistry can be altered by the molar ratio of the materials in the precursor. While these results suggested that it is beneficial

for the device performance when organic cations are present in excess, other works demonstrated that excess lead iodide results in higher PCE.[40,41] The interpretation of these ambiguous findings is further exacerbated by the aging of the precursors in solution. Tsai et al. have shown that the processes of nucleation and growth take place already in the precursor during stirring in solution, and they impact the grain size of the deposited polycrystalline film.[42] These results highlight the multitude and complexity of the parameters affecting the formation of perovskite thin films, and encourages further research aiming to seize control over them.

1.6 Device architectures

Evolving from DSSCs, the first perovskite solar cells were fabricated using a mesoscopic TiO_2 film to extract electrons from the photoactive material. This layout is still the most commonly used for perovskite cells, hence it is often referred to as the standard architecture. With the rapid development of perovskite devices, a wide range of selective charge transport layers and device architectures have been investigated. There are two main device layouts used in perovskite solar cells, differentiated depending on the polarity of the transparent electrode (front contact).

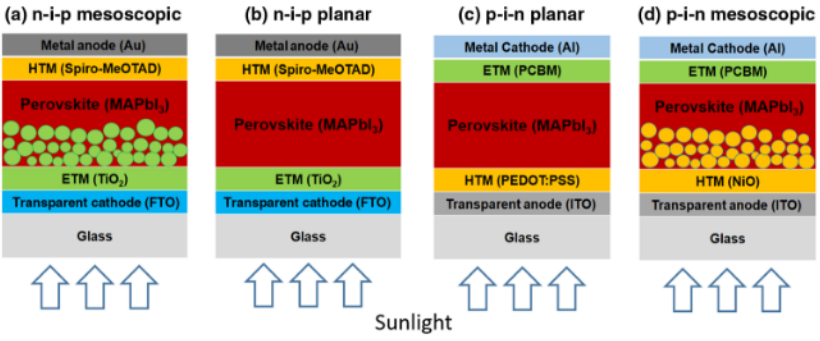

Fig. 5: The most common materials and architectures of perovskite solar cells[43]

When the electron transport layer (ETL) is deposited on the front contact, the device has an n-i-p structure, whereas if the polarity is inverted (holes are extracted at the substrate side), the architecture is called p-i-n. Figure 5 represents the most common materials and architectures used for the fabrication of perovskite solar cells. As the light absorption and hence the photocurrent generation follows an exponential decay as a function of the distance from the surface, one of the charge carrier has to be transported through a longer distance on average before it can be extracted from the photoactive layer. This obviously has implications on device performance, as the diffusion lengths of electrons and holes are usually different. An even more important aspect of the device architecture in solution processed solar cells is the physical and chemical interaction between the perovskite precursor and the underlying layer. An archetypical n-i-p perovskite solar cell uses TiO_2 as the ETL, and spiro-OMeTAD (2,2′,7,7′-tetrakis-(N,N-di-pmethoxyphenylamine)9,9′-spirobifluorene) as the hole transport layer (HTL). While the highest reported power efficiencies were achieved with this type of n-i-p devices, there are a few shortcomings associated with this architecture. To achieve high quality TiO_2 layers, a processing temperature of over 400 °C is needed, which is not compatible with plastic foils and hence complicates the implementation on roll-to-roll processing. Another issue is the frequent presence of hysteresis in the reported J-V scans, which complicates the evaluation of the solar cells photovoltaic performance. One further aspect to be taken account is the poor stability of the spiro-OMeTAD that further impedes the large scale production of solar cells using this material. These challenges have been addressed in several works by developing alternative materials and deposition methods. Perovskite solar cells with a p-i-n architecture use structures similar to those of organic photovoltaics, and as such the typical p-type materials used in this layout are various grades of poly(3,4-ethylenedioxythiophene) polystyrene sulfonate (PEDOT:PSS), while the ETLs are based on fullerene derivatives. These materials have already proven to be scalable and compatible with roll-to-roll fabrication due to their simple and low

temperature processing parameters. However, solar cells based on these materials have so far proven to be slightly inferior compared to their n-i-p counterparts. One possible origin of the losses in Voc and FF is the misalignment of energy levels between the transport layers and the perovskite material. Suns-Voc measurements provide a robust method to understand the contribution of various loss mechanisms in the device – as recently demonstrated by Wu et al, and as such it can be utilized for future device performance optimization.[44]

1.7 Band gap engineering

One of the key features making halide perovskites unique and versatile compounds is the possibility to have their absorption adjusted over a large portion of the electromagnetic spectrum (from about 1 to 3 eV, approximately). Bromide ions are capable of modifying the band gap and photovoltaic performance of solar cells based on the MAPI perovskite – as demonstrated first by Noh et al.[45] In this work, stoichiometric mixtures of MAI and PbI_2 and MABr and $PbBr_2$ were used to fabricate perovskite films with varying band gap. While the absorption onset of the perovskites and the external quantum efficiency (EQE) of the corresponding solar cells demonstrated that a variation of the band gap could be easily achieved, the solar cells performance showed a deviation from the expected behavior. They have observed a decrease in V_{oc} when the Br content was between 0.2 and 0.58, in contrast with the widened perovskite band gap. Furthermore, it was shown that a small amount of Br incorporation improves the humidity resistance of the solar cells. Eperon et al. investigated a system with the composition $FAPb(I_xBr_{1-x})_3$, where FA is the formamidinium cation, varying the ratio between the halide ions.[46] This study has found that the optical band gap energy (E_g) of this system can be tuned between 1.48 and 2.23 eV, however the material is unable to form a pure phase when the Br^- ratio is between $0.5 < x < 0.7$. Following this initial work, several studies aimed at widening the band gap of perovskites via bromide incorporation, however most of the reports observed a limited open-circuit voltage. Hoke et al. investigated this effect in detail and found

that mixed iodide-bromide systems undergo a reversible phase segregation under illumination.[47] This was supported by the appearance of complementary signals in the photoluminescence (PL) spectra and in the x-ray diffraction (XRD) pattern of $MAPb(I_xBr_{1-x})_3$ systems. Slotcavage et al. have shown that the extent of phase separation depends on the illumination intensity (see Fig. 6) with higher fluences having a greater effect.[48] This effect can be alleviated by chemical modification of the perovskite. In particular, complementary A-site cations that impose a strain on the perovskite lattice might help in suppressing this effect.[49] Comparing different works, Slotcavage et al. have postulated that the presence of hysteresis in the current density-voltage (J-V) curves under illumination in perovskite solar cells might also arise from halide migration in the lattice.[48]

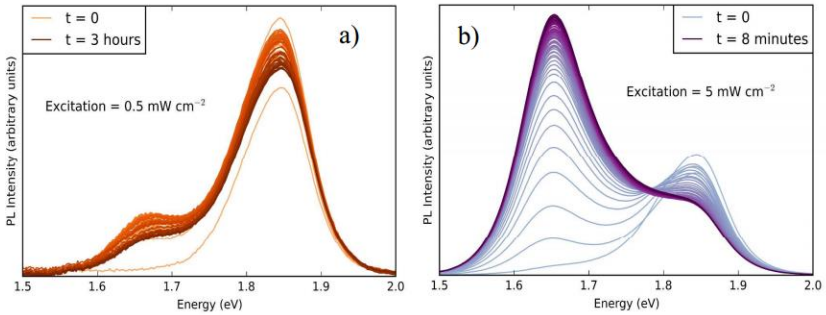

Fig. 6: The evolution the PL of $MAPb(I_{0.6}Br_{0.4})_3$ under different illumination intensities[48]

Besides the efforts to fabricate absorbers with a wider band gap compared to that of pure MAPI, perovskites with a narrower forbidden band energy are also investigated in order to approach the optimal value for single junction solar cells. Exchanging methylammonium cations with formamidinium slightly red-shifts the absorption onset, leading to higher photocurrents.[46] Tin-based and mixed tin-lead perovskites were shown to be a promising candidate to substantially narrow the bandgap as early as in 2013.[50] However, due to the strong tendency of Sn(II) to

oxidize to the tetravalent state, solar cells that incorporated such materials were initially only poorly performing.[51] Later research reported that the addition of SnF_2 successfully suppresses the incorporation of Sn^{4+} ions in the film, paving the way to high performance solar cells using tin-based perovskites as the photoactive material.[52] In 2017, Zhao et al. have demonstrated a low band gap mixed tin-lead perovskite, reaching 17.6% efficiency in a single junction device based on a perovskite absorber with a band gap of 1.25 eV.[53]

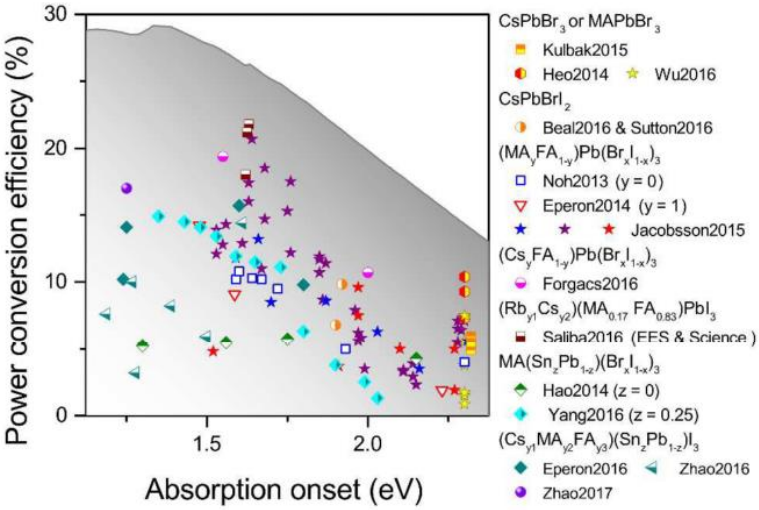

Fig. 7: Efficiency of perovskite solar cells reported in literature as a function of their band gap energy. The grey area represents the Shockley-Queisser limit.[13]

While recent works on band gap engineering have revealed remarkable improvements over the performance of initial devices, there is still of room for improvement. Fig. 7 represents the perovskite solar cells reported in literature, highlighting their efficiency as a function of the band gap of the photoactive layer, and indicates the Shockley-Quessier limit in grey as a benchmark for comparison.

1.8 Tandem solar cells

The record efficiency of the most commercially relevant PV technologies are lately only slowly improving, as they are close to the maximum obtainable performance for single junction solar cells – the Shockley-Queisser limit.[5] The major constraint arises from spectral losses, as most of the available energy cannot be harvested by a single absorber, due to unavoidable carrier thermalisation. The impact of this limitation can be limited through the development of tandem architectures, combining light harvesting semiconductors with complementary absorption spectra. The detailed balance maximum efficiency limit for a 2-terminal tandem cell is 42%, as calculated by De Vos.[54] The graph representing the highest achievable values as a function of the E_g combinations is shown on Fig. 8.

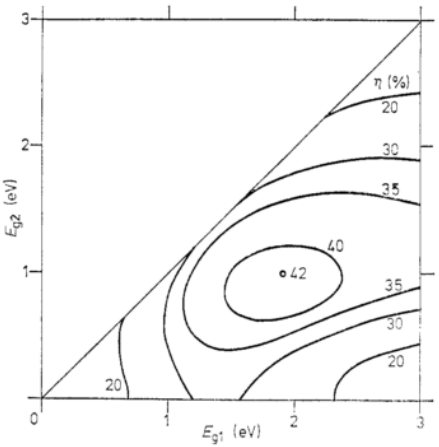

Fig. 8: Maximum achievable PCE in a double junction solar cell utilizing absorbers with a band gap of E_{g1} and E_{g2}[54]

The preparation of a double junction solar cell incorporating commercially available mature technologies, such as crystalline silicon (c-Si) or CIGS solar cells (with band gaps between 1.1 – 1.3 eV), requires a complementary absorber with a band gap between 1.7 – 1.9 eV. While

this approach can improve device efficiency, it also makes the fabrication more complex, which is a crucial subject to consider in the perspective of a viable commercialization. Due to the above mentioned reasons, halide perovskite solar cells are particularly interesting for tandem applications, as their band gap can be engineered by an appropriate choice of the compound stoichiometry, and they also offer low cost fabrication methods combined with high performance. Their exceptional tunability makes them promising candidates to couple with c-Si or CIGS solar cells, and the realization of an efficient perovskite/perovskite tandem holds enormous commercial potential. Tandem solar cells can be either 2-terminal (monolithic) or 4-terminal. In monolithic tandem cells, all the layers are deposited on top of each other in a series connection, while 4-terminal solar cells are in fact two separate photovoltaic devices wired together externally. A problem of 4-terminal tandem cells is the requirement of transparent conductive material, which can be partially alleviated when using monolithic devices. There are, however, several challenges that have to be addressed to manufacture monolithic tandem cells. First of all, the sub cells must have a matching current output for maximum efficiency, otherwise the one outsourcing the lowest current will limit the device performance being the two cells connected in series. This requires a thorough study and computational modelling of each layer, in order to optimize the absorption while guaranteeing an equal photocurrent from the subcells. An additional issue arising in solution processed monolithic tandem cells is the need of solvent orthogonality, as the solvent used to process one layer should not damage the underlying film. Due to these challenges, there have only been a handful of works showing perovskite/perovskite tandem cells, and most of the devices had efficiency inferior to the single cell counterparts. Jiang et al. demonstrated the first bottom up processed perovskite/perovskite tandem cell, utilizing MAPI in both sub cells as the absorber material. With a CRL of spiro-OMeTAD/PEDOT: PSS/PEI/PCBM: PEI, they were able to reach the robustness required to process a second active layer without damaging the first.[55] The V_{oc} of the tandem cell reached

1.89 V, close to the double of the value obtained for the reference single junction cells. It also maintained a reasonably high FF of 56%. This has proven the CRL to be efficient, however the tandem cell was current limited, and hence it was not able to outperform the reference single junction device. Heo et al. have created a tandem cell combining methylammonium lead bromide (MAPBr) and MAPI as the wide and narrow band gap absorber cells respectively.[56]

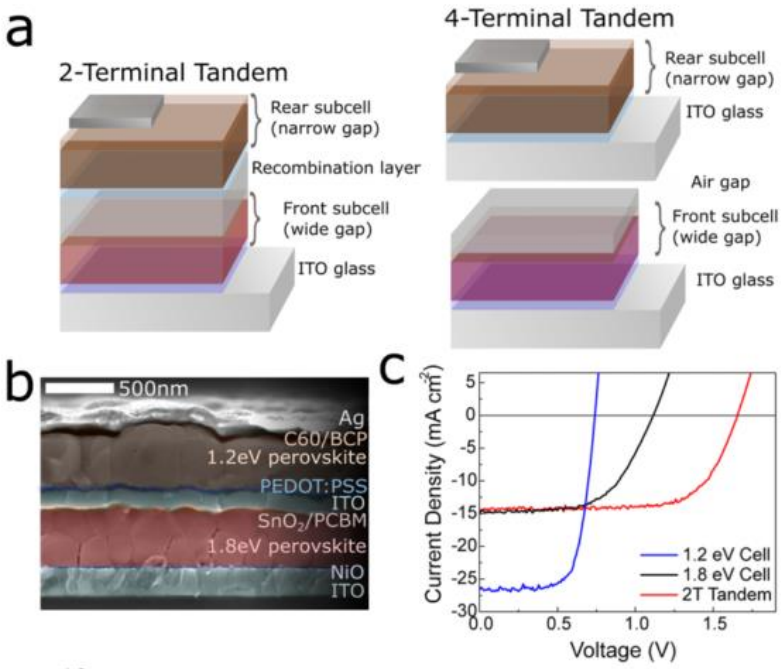

Fig. 9: a) Configurations of a 2 and a 4 terminal tandem solar cell. b) SEM cross section and c) J-V curves of the 2-terminal perovskite/perovskite tandem cells reported by Eperon et al.[57]

The higher voltage of the wide band gap sub cell allowed them to reach a V_{oc} of 2.25 V, however due to photocurrent limitation the tandem cells were still less efficient compared to the reference MAPI device. More recently, Eperon et al. demonstrated 2-terminal perovskite/perovskite

tandem cells with optimized band gaps.[57] Incorporating $FA_{0.75}Cs_{0.25}Sn_{0.5}Pb_{0.5}I_3$ (E_g: 1.2 eV) with the complementary absorber $FA_{0.83}Cs_{0.17}Pb(I_{0.5}Br_{0.5})_3$ (E_g: 1.8 eV), they reached a PCE of 17% in a 2-terminal tandem cell configuration, successfully surpassing the performance of both individual sub cells.

The following chapters will review the research carried out in the thesis in chronological order, highlighting contemporary literature in detail and demonstrating the relevance of the results that have been obtained accordingly.

2 Aim of the thesis

The aim of the thesis was the development of novel materials and device architectures in order to meet different technological challenges.

I. To develop a method that allows the simple and reproducible preparation of efficient perovskite solar cells via solution processing. This is relevant for the future development of perovskite photovoltaics.

II. To investigate various methods to tune the band gap of perovskites and prepare solar cells based on a wide band gap material capable of delivering a high photovoltage. This would allow to prepare tandem cells with complementary absorption, potentially increasing the maximum efficiency that can be obtained using perovskites as the photoactive layer.

III. The final goal is to realize a monolithic tandem solar cell using organic semiconductors as charge transport layers and complementary perovskite absorbers. This is challenging with solely solution processing, as the basic requirement of solvent orthogonality has to be met. Hence both solution and vacuum based methods will be used to achieve this goal.

3 Experimental Methods

3.1 Substrate preparation

Glass substrates with sputtered indium tin oxide (ITO) electrodes were used for the preparation of solar cells. The substrates were first thoroughly rubbed with a water based Mucasol detergent solution, then transferred into a teflon sample holder and then sonicated in the same solution for 5 minutes. After the sonication the residual detergent was washed by copious amounts of tap water followed by rinsing and sonication in MilliQ water. The samples were then sonicated into isopropyl alcohol (IPA) for 5 minutes. The drying was then carried out using a N_2 gun. The substrates were then placed into a UV-O_3 chamber, and treated for 20 minutes to remove any residual organic materials and for surface activation.

3.2 Solution processing of p-i-n solar cells

An 80 nm thick PEDOT:PSS (Clevios PVP AI 4083 from Hereaus) film was deposited in air, and annealed at 130 °C for 15 minutes. The substrates were then transferred to a N_2-filled glovebox. The perovskite precursor solution was filtered and spin-coated on top and the resulting layers were annealed at 90 °C for 20 minutes on a hot plate. The perovskite formation was monitored by recording its UV-Vis absorption spectrum every 5 minutes. A layer of phenyl-C_{61}-butyric acid methyl ester (PCBM) was then deposited from a 2 wt% chlorobenzene solution in air.

3.3 Solution processing of n-i-p solar cells

A 50 nm thick TiO_2 nanoparticles layer (Solaronix Ti-Nanoxide T-L/SC) was deposited in air, at a spinning speed of 6500 rpm for 30 seconds. The contact pads were cleaned with water, and the layers annealed at 200 °C for 30 minutes. The substrates were then transferred to a N_2-filled glovebox. A 10 nm thick indene-C_{60}-propionic acid hexyl ester (IPH) was deposited from a 7.5 mg/mL solution in chlorobenzene at a coating speed of 2000 rpm for 30 seconds, and annealed at 70°C for 10 minutes.[58] The perovskite precursor solution was spin-coated at 1000 rpm for 3 seconds and 2000 rpm for 85 seconds. 5 seconds before finishing the coating, 100 µL of toluene was dripped in the middle of the rotating substrate. The layers were annealed at 70 °C for 30 seconds, then at 100 °C for 30 minutes.

3.4 Evaporation of doped hole transport layers

The samples were transferred to a high vacuum chamber to deposit the hole transport layer (HTL), consisting of 10 nm of N4,N4,N4",N4"-tetra([1,1'-biphenyl]-4-yl)-[1,1':4',1"-terphenyl]-4,4"-diamine (TaTm) and 40 nm of TaTm doped with 2,2′-(perfluoronaphthalene-2,6-diylidene) dimalononitrile (F_6-TCNNQ). The materials are placed into ceramic crucibles fitted into thermal sources with separate power controllers. Three quartz crystal microbalances are allocated inside the chamber – one at each source and one at the substrates - to allow the precise control of the deposition rate. The evaporation is carried out at a pressure of about 10^{-6} mbar.

3.5 Evaporation of metal electrodes

The metal electrodes were thermally evaporated in a high vacuum chamber. The substrates were covered with shadow masks to define the active area of the solar cells. The metal pellets were

placed into a tungsten boat, and current is driven through it in high vacuum to evaporate the material. 10 nm Ba capped with 80 nm Ag in case of p-i-n, and 70 nm of Au in case of n-i-p devices were evaporated at 10^{-6} mbar pressure.

3.6 Solar cell characterization

The external quantum efficiency (EQE) was estimated using the cell response at different wavelength (measured with a white light halogen lamp in combination with band-pass filters), where the solar spectrum mismatch is corrected using a calibrated Silicon reference cell (MiniSun simulator by ECN, the Netherlands). The current density-voltage (J-V) characteristics were obtained using a Keithley 2400 source measure unit in the dark and under white light illumination, and the short circuit current density was corrected taking into account the device EQE. The electrical characterization was validated using a solar simulator by Abet Technologies (model 10500 with an AM1.5G xenon lamp as the light source). Before each measurement, the exact light intensity was determined using a calibrated Si reference diode equipped with an infrared cut-off filter (KG-3, Schott). The J-V characteristics were measured under illumination using a shadow mask to prohibit lateral current collection from outside the active area. The solar simulator provides an AM 1.5G spectrum with an irradiance of 1000 W/m^2, and the shadow has an aperture of 0.01 cm^2.

3.7 UV-Vis spectrometry

The absorbance of thin films was carried out using a fiber optics based Avantes Avaspec2048 spectrometer. After the light source was turned on, a 10 minutes stabilization time allowed the source to reach a stable spectrum. Reference dark and illuminated spectra were recorded, to correct for the background noise and parasitic absorption that might alter the measurement.

Then samples were then placed on the sample holder stage, and their absorption spectra were recorded.

3.8 Photoluminescence (PL) measurements

Photoluminescence measurements were carried out using a continuous green laser with a peak emission at 515 nm and a power of 50 mW. The detector used was the same as for the absorption measurements described above. Reference dark and illuminated spectra were recorded, using a 590 nm long pass filter to avoid the detector saturation with the laser source. The perovskite samples were then placed on the sample holder, and their PL signal was recorded immediately after turning on the laser. The change in the PL signal was monitored by recording an emission spectrum every 30 seconds.

3.9 XRD measurements

The grazing incidence X-ray diffraction (GIXRD) pattern of perovskite thin films were recorded on an Empyrean PANanalytical powder diffractometer using the Cu Kα1 radiation. Typically, three consecutive measurements were collected and averaged into single spectra. The samples were placed on the center of the stage, and the optics were aligned to yield the maximal signal intensity. The scan was carried out in the 2θ range from 5 to 50°.

3.10 AFM measurements

Samples for AFM studies were prepared on pre-cut 1x1 cm glass substrates. The measurements were carried out in tapping mode, using a Multimode SPM microscope (Veeco, USA).

3.11 SEM measurements

Samples for SEM were also prepared on pre-cut 1x1 cm glass substrates. These were placed on a stub of metal with adhesive. Silver ink was used to provide a conductive pathway between the sample and the stub, preventing the overcharging of the sample. Consequently, a thin layer of platinum (< 10 nm) was deposited on top, and it was then transferred to the SEM. Measurements were carried out in various magnifications using a beam voltage of 5 – 20 kV on a Hitachi S-4800 microscope.

4 Lead acetate based perovskite solar cells

Between 2012 and 2014 the number of reports on perovskite solar cells rose rapidly, with continuously increasing maximum efficiency. Most of these findings were rather empirical, as the fundamental chemistry of perovskite precursors were not yet understood, and it was often difficult to reproduce the reported protocols. One major issue that arose through most of the one-step processing methods was that the deposited films were rough and not continuous. This meant that the resulting photovoltaic devices had low parallel resistance, and that thick selective contacts were needed to prevent shunts through the devices. It has been observed how, in PbI_2:MAI stoichiometric solutions (1:1), needle-like lead polyiodide complexes are formed, and these species guide the crystallization resulting in rod-shaped crystals and poor coverage. Buin et al. performed density functional theory (DFT) calculations and found that an I-poor environment is preferred for the growth of perovskite crystalline domains to lower the density of trap states. They correlated these results with the better performance of devices fabricated from $PbCl_2$ based precursors, and postulated that halide-free lead precursors such as $Pb(SCN)_2$ or lead acetate ($Pb(OAc)_2$) might be viable alternatives to achieve high performance perovskite photovoltaics.[59] A simple and reproducible method was developed by Zhang et al., when they used $Pb(OAc)_2$ in the precursor. Methylammonium acetate has a low boiling point, and during annealing it leaves the system rapidly. This shifts the chemical reaction towards the formation of the perovskite phase, leading to rapid nucleation and uniform coverage of the substrate, with a very low surface roughness. It also allows a low temperature processing of the perovskite layer, which is attractive as possible route for large scale production. The highest performance reported in this work was 15.2 % in an n-i-p structure. While the PCE and the morphology achieved were remarkable, the low temperature processability was not applied to its full potential, as the perovskite films were deposited on a compact TiO_2 layer that was previously sintered at 500 °C. Also, the solar cell electrical characteristics presented a remarkable

hysteresis between the forward and reverse J-V curves. Hence it was of great interest to apply this approach to a p-i-n architecture, which is known to have a less pronounced hysteretic behavior and also allows low temperature processing.

The experiments were successful, and the above mentioned goals were achieved. Namely, we have prepared smooth and pinhole-free perovskite layers that show a hysteresis-free and reproducible performance when incorporated into a p-i-n solar cell. The temperature of the heat treatments employed are compatible with processing on plastic foils, making this approach an interesting candidate for roll-to-roll large-scale production.

Journal of Materials Chemistry A

COMMUNICATION

View Article Online
View Journal

Cite this: DOI: 10.1039/c5ta03169a

Received 30th April 2015
Accepted 5th June 2015

DOI: 10.1039/c5ta03169a

www.rsc.org/MaterialsA

Lead acetate precursor based p-i-n perovskite solar cells with enhanced reproducibility and low hysteresis†

Dávid Forgács, Michele Sessolo and Henk J. Bolink*

A low temperature approach for the fabrication of p-i-n perovskite solar cells is presented. Using lead acetate-based precursors, flat and homogeneous $CH_3NH_3PbI_3$ films, compatible with the use of thin organic charge transport layers, can be obtained. The corresponding solar cells showed power conversion efficiency up to 12.5%, with remarkable reproducibility and very low hysteresis.

Photovoltaic devices employing organic–inorganic (hybrid) halide perovskites as the active layer have become a major field of research since the pioneering work by Miyasaka and his co-workers.[1] In the last few years, the power conversion efficiencies (PCEs) of the devices increased from 3.8% to the current record of 20.1%,[2] approaching the performance of mature technologies such as silicon solar cells, and solidifying their place as a possible disruptive technology in the market. Hybrid perovskites possess desired properties for application in photovoltaics, such as high absorption coefficient, wide range of absorption in the visible part of the solar spectrum, direct band gap,[3] long carrier diffusion lengths[4] and the possibility to be produced by solution processing, potentially leading to cheap, large scale, roll-to-roll compatible fabrication. Despite the high reported efficiencies, there are still several issues that need to be addressed before this technology is ready for mass production. One key objective is to develop more reliable and consistent deposition processes.[5,6] It is well understood that the crystalline structure of the perovskite plays a crucial role in the device characteristics.[7,8] Therefore, to successfully fabricate reproducible high performance solar cells, the perovskite crystallization process needs to be controlled either by the appropriate choice of processing parameters, techniques[9] and/or by material selection. For high performance diodes, smooth, trap- and pinhole-free layers with large crystal sizes[10] are desired to allow for thick active layers with good transport properties.[11] With this perspective, different preparation methods have been developed. The perovskite active layer can be deposited by vacuum processing, either by co-,[12–14] sequential-,[15] or flash evaporation,[16] and by solution processing from a precursor solution[17] or a sequential deposition[18] method. In the latter approach, various solvents have been used – *i.e.* dimethylformamide (DMF),[19] dimethylsulfoxide (DMSO),[20] or *N*-methyl-2-pyrrolidone (NMP).[10] Initially, lead iodide and methylammonium iodide had been used to prepare the pure iodide perovskite material, $CH_3NH_3PbI_3$. Soon after, it was demonstrated that by replacing lead iodide with lead chloride, devices with better performances could be obtained.[21] This has been referred to as the mixed halide route, even though the amount of chloride in the final perovskite is negligible.[22] It has been shown that the spectator ion has an effect on the crystal growth kinetics and that, by exchanging the iodide with other anions, the properties of the resulting perovskite layer could be significantly altered. Moore *et al.* compared the crystallization pathways of perovskites obtained from several lead precursors (iodide, chloride, acetate and nitrate) by monitoring the material growth using *in situ* wide-angle X-ray scattering.[23] They have found particularly favourable kinetics when using the lead acetate precursor, *i.e.* long processing windows for obtaining large crystalline perovskite domains at low temperature. This route has been applied in several approaches to explore the possibilities it provides to prepare optoelectronic and photovoltaic devices.[24–26] The highest performance from the latter group is reported by Zhang *et al.*, who prepared perovskite solar cells with the lead acetate precursor and obtained smooth, pinhole-free perovskite films, resulting in devices with a champion PCE of 15.2%.[27] They have used an n-i-p ("standard") device configuration, where the perovskite was deposited onto a compact TiO_2 layer. Such architecture requires a high temperature annealing treatment, and as such it cannot be directly implemented in plastic foils, or in multi-junction devices. Moreover, these solar cells show a pronounced hysteresis during the *J–V* characterisation, making the extraction of the key device parameters somewhat

Instituto de Ciencia Molecular, Universidad de Valencia, c/Catedrático J. Beltrán, 2, 46980 Paterna, Spain. E-mail: henk.bolink@uv.es; Fax: +34-963543273; Tel: +34-963544416

† Electronic supplementary information (ESI) available. See DOI: 10.1039/c5ta03169a

ambiguous. The origin of hysteresis in perovskite solar cells is still under investigation; however, it has been shown to be extremely sensitive to the characterization conditions (scan speed, pre-bias, temperature, *etc.*).[28] Perovskite p-i-n planar heterojunctions have been demonstrated to show less-pronounced hysteresis behaviour, in virtue of a more electronically favourable electron extraction interface.[29,30] With these premises, we have applied the lead acetate precursor route to the fabrication of p-i-n solar cells employing organic semiconductors as charge transport layers. These devices can be prepared at low temperature and are thus more compatible with roll-to-roll fabrication.[31] Here we show that the perovskite layers fabricated by a one-step deposition method from a lead acetate precursor lead to reproducible and efficient p-i-n solar cells with negligible hysteresis *J–V* behaviour.

Device preparation

Methylammonium iodide (MAI) was purchased from Lumtec, lead acetate trihydrate ($Pb(OAc)_2$) was purchased from Aldrich, and both materials were used as received. The substances were mixed in a nitrogen filled glovebox to yield a 40 wt% solution in anhydrous DMF with a 3 to 1 molar ratio of MAI to $Pb(OAc)_2$, and stirred overnight. Glass substrates with an indium-doped tin-oxide (ITO) coating were subsequently cleaned with a detergent solution, Millipore water, isopropyl alcohol, and then transferred to a UV-ozone chamber for 20 minutes of treatment. Afterwards, 80 nm thick poly(3,4-ethylenedioxythiophene) doped with poly(styrenesulfonate) (PEDOT:PSS, Clevios PVP AI 4083 from Hereaus) film was deposited in air, and annealed at 130 °C for 15 minutes. The substrates were then transferred to a N_2-filled glovebox. The perovskite precursor solution was filtered and spin-coated on top and the resulting layers were annealed at 90 °C on a hot plate. The perovskite formation was monitored by recording the UV-Vis spectrum every 5 minutes. A layer of phenyl-C61-butyric acid methyl ester (PCBM) was then deposited from a 2 wt% chlorobenzene solution, and the metal contacts (10 nm Ba capped with 80 nm Ag) were thermally evaporated on top. Device characterization was performed using a mini-sun simulator with a halogen lamp designed by ECN and calibrated with a Si reference cell. The unencapsulated solar cells were analysed in a N_2-filled glovebox. The current density (*J*) *versus* voltage (*V*) characteristics were measured in the dark and under illumination using a shadow mask to prohibit lateral current collection from outside the active area.

Results and discussion

The evolution of the pristine precursor layers was followed by an optical absorption measurement, monitoring the band-edge transition of the $CH_3NH_3PbI_3$ perovskite. Interestingly, the typical strong, broad absorption centered between 750 and 775 nm was already observed after only 5 minutes annealing at 90 °C (Fig. 1a), in accordance with the favourable formation kinetics of the perovskite from the lead acetate precursor. Longer annealing resulted in only a slight increase of the absorption at the bandgap energy, and after 20 minutes no change could be observed, suggesting the quantitative conversion of the precursor compound to $CH_3NH_3PbI_3$. The crystallinity of the perovskite was investigated by grazing incidence X-ray diffraction (GIXRD) measurements, revealing the pattern (in terms of both the peak position and relative intensity[20]) of a typical pure-iodide perovskite (Fig. 1b). One sample was continuously measured in air and, after approximately 10 hours, the diffraction peak of lead iodide appeared and started to grow (see ESI†), indicating the decomposition of the perovskite due to the presence of oxygen and moisture.

The $CH_3NH_3PbI_3$ perovskite layers were further characterized by atomic force microscopy (AFM) and scanning electron microscopy (SEM), in order to investigate their surface morphology and structure. The AFM topography (Fig. 2a) revealed a homogeneous surface composed of closely packed, fine grains.

The corresponding root mean squared roughness, calculated over an area of 25 μm^2, was found to be 19.05 nm. This indicates a very smooth surface, and allows the use of thin organic selective layers to sufficiently cover the perovskite material and

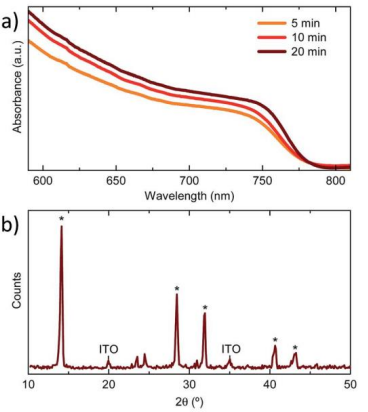

Fig. 1 UV-Vis absorption (a) of a perovskite thin film with increasing annealing time at 90 °C. GIXRD spectra (b) of the thin film after annealing for 20 minutes. The characteristic diffraction peaks as well as those arising from the ITO substrate are highlighted.

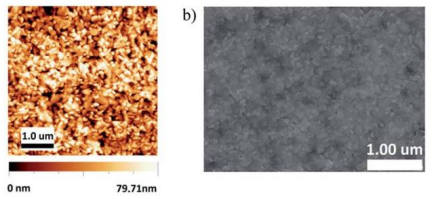

Fig. 2 AFM topography (a) and SEM (b) image of the perovskite surface deposited on ITO/PEDOT:PSS.

prevent surface recombination at the top metal contact. SEM analysis (Fig. 2b) confirms the homogeneous and pinhole-free film morphology, with grain sizes of approximately 100 nm in diameter. Perovskite solar cells, with the structure ITO/PEDOT:PSS/$CH_3NH_3PbI_3$/PCBM/Ba–Ag, were fabricated following the previously described method. The *J–V* curves were recorded between −0.2 and 1.2 V with 0.01 V steps, integrating the signal for 20 ms after a 20 ms delay. This corresponds to a speed of 250 mV s^{-1} which is similar to that used by Zhang *et al.* in their work, allowing a direct comparison between their n-i-p and our p-i-n architecture.[27] We have extended the range to even lower scan speeds, where the hysteresis becomes even smaller (see Fig. S2 in the ESI†). Generally, pixels on the same substrate (area of 9 cm^2) have very similar performances, independent of the position. This fact highlights the potential of this deposition route for large-area solution processing of perovskite cells. To stress the homogeneity of the layers, the *J–V* curves corresponding to four pixels (0.0264 cm^2) on the same substrate are reported in Fig. 3a, and the corresponding figures of merit are shown in Table 1. The open circuit voltage V_{oc} varies in the range of 950–960 mV, which is slightly lower compared to what is commonly observed in high efficiency perovskite solar cells, but in agreement with a previous study using the same lead precursor.[27]

The recorded short circuit current density J_{sc} and FF values are 18–19 mA cm^{-2} and 65–70%, respectively. The champion device prepared by this approach exhibited a PCE of 12.5%. The thickness of the active layer measured with a mechanical profilometer was approximately 300 nm. Such a thickness enables high light harvesting and allows the charges to leave the active layer before recombining, as demonstrated by the high external quantum efficiency (EQE, inset of Fig. 3a). Thicker layers would increase the absorption and charge generation, so that devices with higher photocurrents could be realized. However, we have observed a decrease in the fill factor and hence in the device performance for perovskite layer thicknesses exceeding 300 nm. This is most likely due to the morphology of the active layer, which is composed of fine grains of approximately 100 nm in size. While these dimensions result in a flat and homogeneous film surface, they might hinder efficient extraction of charges from thick active layers.[10] During the *I–V* measurements, virtually no hysteresis was observed between the curves recorded in forward (negative to positive) and reverse (positive to negative) biases. J_{sc} and V_{oc} show less than 1% difference between the forward and reverse scans in all measured devices. The FF is in general slightly higher in the reverse scan, in agreement with most reports on hybrid perovskite solar cells, and it is independent of the precursor material or processing method.[27,29,32]

Table 1 Device parameters from the *J–V* curves depicted in Fig. 3a

Forward scan			
V_{oc} (mV)	J_{sc} (mA cm^{-2})	FF (%)	PCE (%)
960	18.2	67.4	11.8
953	18.1	65.5	11.3
958	18.9	66.0	11.9
956	18.8	69.0	12.4
Reverse scan			
V_{oc} (mV)	J_{sc} (mA cm^{-2})	FF (%)	PCE (%)
963	18.2	67.6	11.8
953	18.1	66.4	11.5
957	18.9	66.9	12.1
954	18.8	69.7	12.5

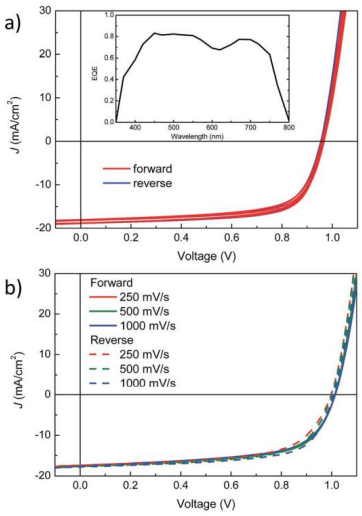

Fig. 3 *J–V* curves of 4 pixels on the same substrate (a), in forward and reverse scans. The inset shows the EQE of the best performing device. Forward and reverse *J–V* curves of another set of solar cells measured at different scan rates (b).

The difference remains rather small, being less than 5% of the measured value for all devices. To further investigate the effect of hysteresis, measurements were carried out using different scan speeds (Fig. 3b). We observed very limited hysteresis regardless of the scan rate, with only the FF slightly varying while leaving the V_{oc} and J_{sc} values unchanged. A total of 48 devices were fabricated using this configuration and method. The PCEs recorded at 250 mV s^{-1} ranged from 10.2% to 12.5%, which is a fairly narrow distribution, further demonstrating the reproducibility of this approach. Fig. 4 shows the histogram of the obtained PCE values with an overlaid normal distribution function. Hence, independently of the scanning speed and direction, and consistency over different devices, the *J–V* characteristics of the solar cells are rather similar, making this approach promising for future optimization and device physics analysis.

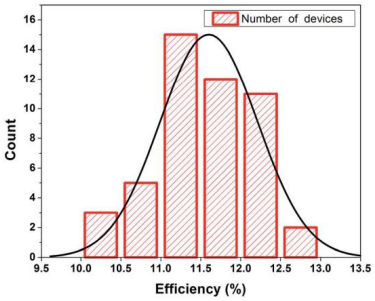

Fig. 4 Device efficiency histogram with an overlaid distribution function.

Conclusions

We have investigated the effect of an alternative precursor, lead acetate, on the preparation of p-i-n (inverted) perovskite solar cells. The obtained perovskite layers are smooth and pinhole-free over a large area, therefore are suitable for use in combination with thin organic semiconducting transport layers. Solar cells exhibit a remarkably low hysteresis which is also independent of the scan speed. Moreover, the device performances are consistent and remain within a fairly narrow range, indicating the reproducibility of this approach. Finally, device processing does not involve any high temperature treatment, thus making this approach a good candidate for flexible device fabrication and for the preparation of monolithic tandem perovskite solar cells.

Acknowledgements

This work has been supported by the Spanish Ministry of Economy and Competitiveness (MINECO) (MAT2011-55200), and the Generalitat Valenciana (Prometeo/2012/053).

References

1 A. Kojima, K. Teshima, Y. Shirai and T. Miyasaka, *J. Am. Chem. Soc.*, 2009, **131**, 6050–6051.
2 H. S. Jung and N.-G. Park, *Small*, 2015, **11**, 10–25.
3 W.-J. Yin, J.-H. Yang, J. Kang, Y. Yan and S.-H. Wei, *J. Mater. Chem. A*, 2015, **3**, 8926–8942.
4 D. Shi, V. Adinolfi, R. Comin, M. Yuan, E. Alarousu, A. Buin, Y. Chen, S. Hoogland, A. Rothenberger, K. Katsiev, Y. Losovyj, X. Zhang, P. A. Dowben, O. F. Mohammed, E. H. Sargent and O. M. Bakr, *Science*, 2015, **347**, 519–522.
5 H. J. Snaith, A. Abate, J. M. Ball, G. E. Eperon, T. Leijtens, N. K. Noel, S. D. Stranks, J. T.-W. Wang, K. Wojciechowski and W. Zhang, *J. Phys. Chem. Lett.*, 2014, **5**, 1511–1515.
6 J. A. Christians, J. S. Manser and P. V. Kamat, *J. Phys. Chem. Lett.*, 2015, **6**, 852–857.
7 Y. Tidhar, E. Edri, H. Weissman, D. Zohar, G. Hodes, D. Cahen, B. Rybtchinski and S. Kirmayer, *J. Am. Chem. Soc.*, 2014, **136**, 13249–13256.
8 P.-W. Liang, C.-Y. Liao, C.-C. Chueh, F. Zuo, S. T. Williams, X.-K. Xin, J. Lin and A. K.-Y. Jen, *Adv. Mater.*, 2014, **26**, 3748–3754.
9 Z. Xiao, Q. Dong, C. Bi, Y. Shao, Y. Yuan and J. Huang, *Adv. Mater.*, 2014, **26**, 6503–6509.
10 W. Nie, H. Tsai, R. Asadpour, J.-C. Blancon, A. J. Neukirch, G. Gupta, J. J. Crochet, M. Chhowalla, S. Tretiak, M. A. Alam, H.-L. Wang and A. D. Mohite, *Science*, 2015, **347**, 522–525.
11 A. Buin, P. Pietsch, J. Xu, O. Voznyy, A. H. Ip, R. Comin and E. H. Sargent, *Nano Lett.*, 2014, **14**, 6281–6286.
12 O. Malinkiewicz, A. Yella, Y. H. Lee, G. M. Espallargas, M. Graetzel, M. K. Nazeeruddin and H. J. Bolink, *Nat. Photonics*, 2014, **8**, 128–132.
13 M. Liu, M. B. Johnston and H. J. Snaith, *Nature*, 2013, **501**, 395–398.
14 L. Gil-Escrig, G. Longo, A. Pertegas, C. Roldan-Carmona, A. Soriano, M. Sessolo and H. J. Bolink, *Chem. Commun.*, 2015, **51**, 569–571.
15 C.-W. Chen, H.-W. Kang, S.-Y. Hsiao, P.-F. Yang, K.-M. Chiang and H.-W. Lin, *Adv. Mater.*, 2014, **26**, 6647–6652.
16 D. B. Mitzi, M. T. Prikas and K. Chondroudis, *Chem. Mater.*, 1999, **11**, 542–544.
17 F. Wang, H. Yu, H. Xu and N. Zhao, *Adv. Funct. Mater.*, 2015, **25**, 1120–1126.
18 S. A. Kulkarni, T. Baikie, P. P. Boix, N. Yantara, N. Mathews and S. Mhaisalkar, *J. Mater. Chem. A*, 2014, **2**, 9221–9225.
19 J.-Y. Jeng, Y.-F. Chiang, M.-H. Lee, S.-R. Peng, T.-F. Guo, P. Chen and T.-C. Wen, *Adv. Mater.*, 2013, **25**, 3727–3732.
20 Y. Wu, A. Islam, X. Yang, C. Qin, J. Liu, K. Zhang, W. Peng and L. Han, *Energy Environ. Sci.*, 2014, **7**, 2934–2938.
21 M. M. Lee, J. Teuscher, T. Miyasaka, T. N. Murakami and H. J. Snaith, *Science*, 2012, **338**, 643–647.
22 S. Colella, E. Mosconi, P. Fedeli, A. Listorti, F. Gazza, F. Orlandi, P. Ferro, T. Besagni, A. Rizzo, G. Calestani, G. Gigli, F. D. Angelis and R. Mosca, *Chem. Mater.*, 2013, **25**, 4613–4618.
23 D. T. Moore, H. Sai, K. W. Tan, D.-M. Smilgies, W. Zhang, H. J. Snaith, U. Wiesner and L. A. Estroff, *J. Am. Chem. Soc.*, 2015, **137**, 2350–2358.
24 Y. Fu, F. Meng, M. B. Rowley, B. J. Thompson, M. J. Shearer, D. Ma, R. J. Hamers, J. C. Wright and S. Jin, *J. Am. Chem. Soc.*, 2015, **137**, 5810–5818.
25 F. K. Aldibaja, L. Badia, E. Mas-Marzá, R. S. Sánchez, E. M. Barea and I. Mora-Sero, *J. Mater. Chem. A*, 2015, **3**, 9194–9200.
26 H. Zhu, Y. Fu, F. Meng, X. Wu, Z. Gong, Q. Ding, M. V. Gustafsson, M. T. Trinh, S. Jin and X.-Y. Zhu, *Nat. Mater.*, 2015, **14**, 636–642.
27 W. Zhang, M. Saliba, D. T. Moore, S. K. Pathak, M. T. Horantner, T. Stergiopoulos, S. D. Stranks, G. E. Eperon, J. A. Alexander-Webber, A. Abate,

A. Sadhanala, S. Yao, Y. Chen, R. H. Friend, L. A. Estroff, U. Wiesner and H. J. Snaith, *Nat. Commun.*, 2014, **6**, 6142.
28 W. Tress, N. Marinova, T. Moehl, S. M. Zakeeruddin, M. K. Nazeeruddin and M. Grätzel, *Energy Environ. Sci.*, 2015, **8**, 995–1004.
29 J. H. Heo, H. J. Han, D. Kim, T. K. Ahn and S. H. Im, *Energy Environ. Sci.*, 2015, **8**, 1602–1608.
30 P.-W. Liang, C.-C. Chueh, S. T. Williams and A. K.-Y. Jen, *Adv. Energy Mater.*, 2015, **5**, 1402321.
31 J. You, Z. Hong, Y. M. Yang, Q. Chen, M. Cai, T.-B. Song, C.-C. Chen, S. Lu, Y. Liu, H. Zhou and Y. Yang, *ACS Nano*, 2014, **8**, 1674–1680.
32 N. J. Jeon, J. H. Noh, W. S. Yang, Y. C. Kim, S. Ryu, J. Seo and S. I. Seok, *Nature*, 2015, **517**, 476–480.

5 Wide bandgap perovskite solar cells

Since the demonstration of the possibility to simply tune the band gap of perovskites by halide exchange, there have been several attempts to engineer these materials with specific light harvesting properties. As the band gap of around 1.55 eV of MAPI perovskite is much wider than 1.1 eV, which is the optimum required for the maximum achievable efficiency calculated by Shockley and Queisser for single cells, a first approach is to lower the band gap to reach the highest possible power output.[5] On the other hand, a larger bandgap of about 1.75 eV is suitable for a Si/perovskite tandem cell.[54] Researchers have found that the incorporation of various ions have a different effect on the optical properties, the processing possibilities, and the stability of the resulting material. FA cations have been shown to reduce the band gap and provide better thermal resistance, however, as the cation is larger than MA, it requires higher temperature annealing treatments in order to overcome the activation energy and be integrated into the crystal lattice. Cs cations in turn are smaller than MA, and their incorporation leads to wider band gaps and improved moisture and thermal resistance. Exchanging I for Br leads to a larger band gap, as well as improved device stability. However, as several works have pointed out, the mixed halide perovskite $MAPb(I_{1-x}Br_x)_3$ is not stable under illumination when the Br content is between 0.2 and 0.6. With the introduction of the anti-solvent method, it has become relatively easy to test new formulations with a consistent homogeneous morphology. Hence, efficient and stable solar cells have been fabricated employing perovskite films with different optical absorption properties. Most of these works were aimed at enlarging the absorption towards the infrared part of the solar spectrum to achieve high-efficiency single cells, or to develop perovskites with a band gap that is suitable in a sub-cell for a Si/perovskite tandem cell. On the contrary, limited studies have been dedicated to the development of perovskite/perovskite tandem, due to the aforementioned difficulties regarding the device

processing, and the photo-instability of mixed I – Br systems. Hence its investigation remains an important and uncharted area for further development of perovskite photovoltaics.

In our work, we aimed to create a wide band gap perovskite that is suitable as a sub-cell for a tandem device that uses MAPI as its narrow band gap absorber. We tested a series of compositions with the formula $Cs_{0.15}FA_{0.85}Pb(Br_xI_{1-x})_3$ using the anti-solvent method in an n-i-p device architecture. We have chosen to optimize $Cs_{0.15}FA_{0.85}Pb(Br_{0.7}I_{0.3})_3$ due to its optical band gap of around 2.0 eV that is close to optimal in conjunction with a 1.55 eV narrow band gap subcell. By employing a partially solution processed and partially vacuum deposited device architecture, we were able to fabricate efficient solar cells with the desired absorption properties. Even though our PL studies have shown that the photo-instability is not eliminated even in presence of Cs and FA cations, we were able to fabricate the most efficient perovskite photovoltaic device reported to date with a band gap higher than 1.8 eV. Of particular importance is the achievement of large V_{oc} (larger than the MAPI based devices) and very high fill factor (FF), which indicates that this perovskite formulation might allow for a net gain in efficiency with respect to single junction devices, when incorporated in a tandem architecture.

Journal of Materials Chemistry A

COMMUNICATION

View Article Online
View Journal | View Issue

Cite this: J. Mater. Chem. A, 2017, 5, 3203

Received 13th December 2016
Accepted 25th January 2017

DOI: 10.1039/c6ta10727c

rsc.li/materials-a

Efficient wide band gap double cation – double halide perovskite solar cells†

Dávid Forgács, Daniel Pérez-del-Rey, Jorge Ávila, Cristina Momblona, Lidón Gil-Escrig, Benedikt Dänekamp, Michele Sessolo* and Henk J. Bolink

In this work we study the band gap variation and properties of the perovskite compound $Cs_{0.15}FA_{0.85}Pb(Br_xI_{1-x})_3$ as a function of the halide composition, with the aim of developing an efficient complementary absorber for $MAPbI_3$ in all-perovskite tandem devices. We have found the perovskite stoichiometry $Cs_{0.15}FA_{0.85}Pb(Br_{0.7}I_{0.3})_3$ to be a promising candidate, thanks to its band gap of approximately 2 eV. Single junction devices using this perovskite absorber lead to a maximum PCE of 11.5%, among the highest reported for solar cells using perovskites with a band gap wider than 1.8 eV.

Organic–inorganic (hybrid) perovskite solar cells have attracted much attention among the emerging photovoltaic technologies due to the unique properties of the photoactive material. These include high absorption coefficients,[1,2] sharp optical band edges,[3] low exciton binding energies,[4] and long carrier diffusion lengths.[5] The reported efficiency of the solar cells increased rapidly from 3.8% in 2009 to the current certified record of 22.1%,[6,7] making perovskites the fastest evolving photovoltaic technology to date. Previous studies mainly explored different methods to deposit methylammonium lead iodide ($MAPbI_3$) thin films, for instance changing the solvents,[8–10] the precursor compounds[11–16] or the type and number of processing steps used to prepare the absorber layer,[17–20] in order to yield an improved morphology and hence better performing solar cells. Besides single junction devices, one can substantially improve the efficiency of perovskite solar cells by developing tandem architectures with complementary absorbers. The most studied system is perovskite-on-silicon, as it relies on an already established technology and the most studied perovskite absorber, $MAPbI_3$, has a close to optimal bandgap for this application.[21,22] Perovskite–perovskite tandem devices, in which both absorbers are based on perovskite materials, are also being investigated since they can surpass the efficiency of single junction cells.[23,24] In these reports the tandem cell efficiency does not yet surpass that of the single junction devices, due to underperforming wide bandgap cells. In order to fabricate an efficient perovskite–perovskite tandem using $MAPbI_3$ as the low band gap photoactive material, an efficient absorber with a band gap of about 2 eV is needed for the front cell. The development of high performance solar cells employing these materials would also pave the way to fabricate triple junction all-perovskite devices. However, most reports describing efforts to tune the band gap of perovskite absorbers beyond 1.8 eV (*via* mixing Br^- and I^- ions), led to rather poor performing solar cells. Kulkarni *et al.* used a sequential deposition method to vary the ratio of iodide and bromide ions in the perovskite film, demonstrating a steadily tunable optical band gap ranging from 1.56 eV for the pure $MAPbI_3$ to 2.23 eV for the pure $MAPbBr_3$.[25] The devices prepared from these films however did not show the expected increasing open-circuit voltage (V_{oc}) for wider band gaps, and the overall efficiency was low. The highest PCE demonstrated so far for a mixed halide perovskite with 2 eV bandgap, $MAPbIBr_2$, is 4.6%, limited by a low FF and open-circuit voltage (<1 V).[26] By replacing the methylammonium cation with cesium, the inorganic perovskite $CsPbBrI_2$ with a band gap of 1.9 eV, has been employed in solar cells with a maximum PCE of 6.8%, where this low efficiency was due to a hindered charge extraction resulting in a low FF.[27] Jaysankar *et al.* studied the mixed halide $MAPb(I_{0.6}Br_{0.4})_3$ that has a smaller bandgap of 1.77 eV, which is suitable for tandem cells with silicon. After fine-tuning the crystallization dynamics, they demonstrated solar cells with a maximum efficiency of 10.6%.[28] Hoke *et al.* studied mixed halide systems through photoluminescence (PL), and found that a wide range of mixed halide perovskite compositions undergo a reversible photoinduced phase separation, with a new PL peak appearing at a similar wavelength independent of the initial material composition.[29] This arises from the formation of iodide-rich domains with a narrower band gap that likely limits the maximum obtainable V_{oc} of the solar cells based on such materials. This behavior has

Instituto de Ciencia Molecular, Universidad de Valencia, c/Catedrático J. Beltrán, 2, 46980 Paterna, Spain. E-mail: henk.bolink@uv.es; Fax: +34-963543273; Tel: +34-963544416

† Electronic supplementary information (ESI) available. See DOI: 10.1039/c6ta10727c

been reported in several studies in which different preparation methods and compositions were explored to tune the band gap by exchanging I^- with Br^-.[30] It has been shown that there is a miscibility limit which leads to photoinstability and phase separation if the Br^- content is larger than 0.2. This miscibility limit can be overcome at least partially by incorporating Cs^+ and FA^+ ions in the perovskite lattice, yet is not clear to what extent. Saliba *et al.* reported a triple-cation mixed halide low bandgap (1.6 eV) perovskite that reaches a stabilized power output of 21.1%.[31] Using a similar approach but with an increased bromide content of 0.4, McMeekin *et al.* designed a perovskite absorber with a bandgap of 1.74 eV, making it suitable to be efficiently applied to a silicon cell in a tandem architecture, while also providing higher voltage output compared to the triiodide perovskites.[32] In this work, we combine the beneficial stabilizing effects of Cs^+ and FA^+ cations to tune the band gap of the $Cs_{0.15}FA_{0.85}Pb(Br_xI_{1-x})_3$ perovskite to values larger than 2.0 eV. We observe how the photovoltage of the solar cells increases with wider band gaps, however, the gain is not as much as one would expect. This is attributed to the presence of an iodide-rich phase, which is observed by photoluminescence measurements. Hence, also for the Cs^+ and FA^+ containing mixed halide perovskites a miscibility limit exists, for bromide contents higher than 0.4. Yet by optimizing the processing conditions we were able to obtain perovskite solar cells with a bandgap of 2 eV and efficiencies as high as 11.5%, the highest reported to date for devices using light-harvesters with a band gap wider than 1.8 eV.

Device preparation

Formamidinium iodide (FAI) and formamidinium bromide (FABr) were purchased from Dyesol, cesium iodide (CsI), cesium bromide (CsBr), lead iodide (PbI_2) and lead bromide ($PbBr_2$) were purchased from Tokyo Chemical Industry. The precursors and devices were prepared following previously published methods.[32] Briefly, the perovskite precursor materials were mixed in a nitrogen filled glovebox to yield a 1 M solution of $Cs_{0.15}FA_{0.85}PbBr_3$ and $Cs_{0.15}FA_{0.85}PbI_3$, in anhydrous dimethyl sulfoxide (DMSO), and stirred at 60 °C until complete dissolution. The solutions were then mixed by varying volumes to yield the desired iodide to bromide ratio. Glass substrates with an indium tin-oxide (ITO) coating were subsequently cleaned in a detergent solution, Millipore water, and isopropanol, and then activated in a UV-ozone chamber for 20 minutes. After the surface treatment, a 50 nm thick TiO_2 layer (Solaronix Ti-Nanoxide T-L/SC) was deposited in air, at a spinning speed of 6500 rpm for 30 seconds. The contact pads were cleaned with water, and the layers annealed at 200 °C for 30 minutes. The substrates were then transferred to a N_2-filled glovebox. A 10 nm thick indene-C_{60}-propionic acid hexyl ester (IPH) was deposited from a 7.5 mg mL^{-1} solution in chlorobenzene at a coating speed of 2000 rpm for 30 seconds, and annealed at 70 °C for 10 minutes.[33] The optimized process for the deposition of $Cs_{0.15}FA_{0.85}Pb(Br_{0.7}I_{0.3})_3$ perovskite was the following. The precursor solution was spin-coated at 1000 rpm for 3 seconds and 2000 rpm for 85 seconds. 5 seconds before finishing the coating, 100 μL of toluene was dripped in the middle of the rotating substrate. The layers were annealed at 70 °C for 30 seconds, and then at 100 °C for 30 minutes. The samples were then transferred to a high vacuum chamber to deposit the hole transport layer (HTL), consisting of 10 nm of *N*4,*N*4,*N*4″,*N*4″-tetra([1,1′-biphenyl]-4-yl)-[1,1′:4′,1″-terphenyl]-4,4″-diamine (TaTm) and 40 nm of TaTm doped with 2,2′-(perfluoronaphthalene-2,6-diylidene)dimalononitrile (F_6-TCNNQ).[34] Gold was deposited as the top electrode. The devices were then measured under an AM 1.5G spectrum with an irradiance of 1000 W m^{-2}, with a shadow mask (aperture: 0.01 cm^2) to prohibit lateral current collection from outside the active area.

Results and discussion

Mixed cation perovskite layers with varying bromide to iodide ratios were deposited on glass/ITO/TiO_2/IPH substrates. The GIXRD analysis revealed a perovskite structure in all of the compositions studied (see Fig. S1†), with the peak positions shifting to wider angles with increasing bromide content, due to the change in the cubic lattice constant. This proved that the material can crystallize without structural instability, in agreement with previous reports.[32] To test the performance of the perovskite as a function of Br/I ratio, a series of solar cells were fabricated and their external quantum efficiency (EQE) and current–voltage characteristics (*J*–*V* curves) were measured. Fig. 1a shows the UV-Vis absorption spectra of $Cs_{0.15}FA_{0.85}Pb(Br_xI_{1-x})_3$ with a bromide content in the range of $0.7 \leq x \leq 1$, and Fig. 1b the EQE curves of the best performing cells for each composition. With increasing bromide content, the absorption onset gradually shifts to higher energies, and the excitonic peak becomes more pronounced. The EQE of the corresponding solar cells follows the trend in absorption, and the measurements reveal that a large fraction (between 70 and 90%) of the photogenerated charge carriers can be collected regardless of the composition of the perovskite absorber. The short-circuit current density (J_{sc}) values calculated from the EQE measurements, and the V_{oc} of the prepared devices are reported in Fig. 1c (see Fig. S2† for the *J*–*V* curves). The trends in photovoltaic parameters as a function of the perovskite bandgap, such as decreasing V_{oc} and increasing generated photocurrent, are clearly observable. It is important to note that the optimal processing parameters change for each composition, and hence the performance of the devices shown here could certainly be further improved. To achieve 2-terminal monolithic tandem cells that perform better than a single cell, one needs current matched sub-cells, among many other requirements, which in the case of a double junction is optimally about 50% of the current density of what a high performance single junction cell can deliver alone. As high efficiency $MAPbI_3$ solar cells typically generate a J_{sc} between 20 and 24 mA cm^{-2}, we optimized the deposition process for the perovskite composition $Cs_{0.15}FA_{0.85}Pb(Br_{0.7}I_{0.3})_3$, being the absorber with the highest achievable current density. Table 1 shows the statistics of the performance extracted from 20 devices prepared with the optimized processing conditions.

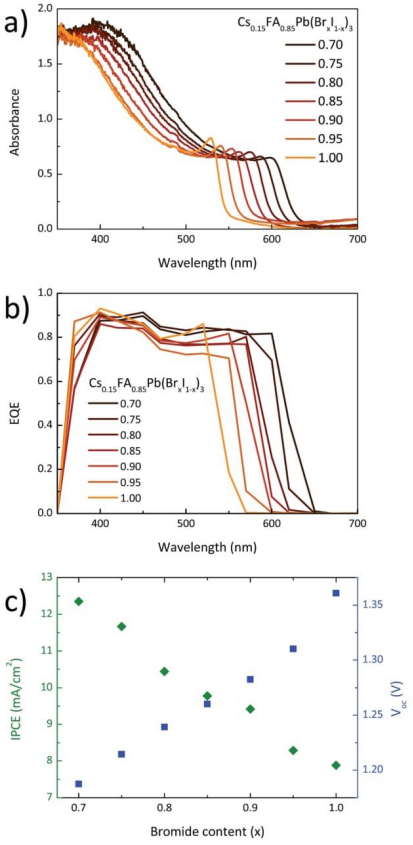

Fig. 1 (a) UV-Vis absorption and (b) EQE spectra of $Cs_{0.15}FA_{0.85}Pb(Br_xI_{1-x})_3$ thin films. The different colours represent the fraction of bromide ions relative to the total halide content. (c) V_{oc} (blue) and IPCE (green) extracted from solar cells based on $Cs_{0.15}FA_{0.85}Pb(Br_xI_{1-x})_3$ as a function of their Br^- content.

Table 1 Statistics on the performance of 20 solar cells based on the $Cs_{0.15}FA_{0.85}Pb(Br_{0.7}I_{0.3})_3$ absorber and prepared with the optimized processing conditions

	Average	SD	Min.	Max.
V_{oc} (mV)	1183	±15	1158	1208
J_{sc} (mA cm^{-2})	11.36	±0.75	9.81	12.47
FF (%)	77.4	±2.2	71.1	80.3
PCE (%)	10.4	±0.6	9.2	11.5

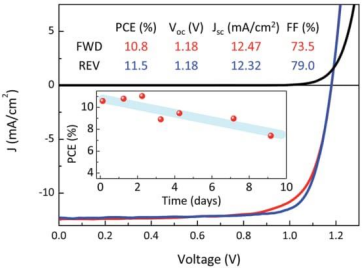

Fig. 2 J–V curves in the dark and under illumination of the best performing device. The inset shows the PCEs of unencapsulated solar cells left under ambient conditions and measured regularly. The data shown are extracted from reverse J–V curves recorded after 15 minutes of illumination.

The data shown suggest that the reported method is reproducible, and generally yields efficient solar cells. The J–V curves in the dark and under illumination for the best performing device are also reported on Fig. 2. We observed a small hysteresis in the J–V curve depending on the scan direction, a phenomenon that is often observed in perovskite solar cells employing TiO_2.[35] Regardless, the photovoltage measured for the mixed halide perovskite cell is higher than its pure iodide counterparts. This feature, together with the high FF and close to optimal J_{sc}, results in a PCE as high as 11.5%, among the highest demonstrated until now for perovskite solar cells with a band gap wider than 1.8 eV.

To test the stability of the perovskite absorber in this device architecture, an unencapsulated solar cell was left under ambient conditions, and J–V measurements were performed over time to track the degradation. We noticed that the solar cells exposed to ambient conditions showed slightly reduced performances during the first measurements, but it gradually recovered under continuous illumination (see Fig. S3†). Hence, the protocol established to track the degradation was to leave the device under 1 sun illumination for 15 minutes, then record a J–V scan in the reverse direction. The inset of Fig. 2 depicts the PCE values obtained as a function of time under ambient conditions. After the first two days, when a small increase of the PCE is observed, the power conversion efficiency starts to diminish, mainly caused by a loss in fill factor. This phenomenon could possibly arise from the de-doping of the HTM deposited on top of the perovskite, leading to the formation of an energy barrier for hole extraction. Besides the favourable properties of the solar cells, there is still a large difference between the optical band gap of the perovskite (about 2 eV in the case of $Cs_{0.15}FA_{0.85}Pb(Br_{0.7}I_{0.3})_3$) and the measured V_{oc}. In order to investigate the origin of this phenomenon, photoluminescence measurements on the perovskite thin films were performed. The excitation source used was a continuous wave green laser, with an emission peak at 515 nm and a power of 50 mW. Fig. 3 represents the PL spectra recorded immediately after

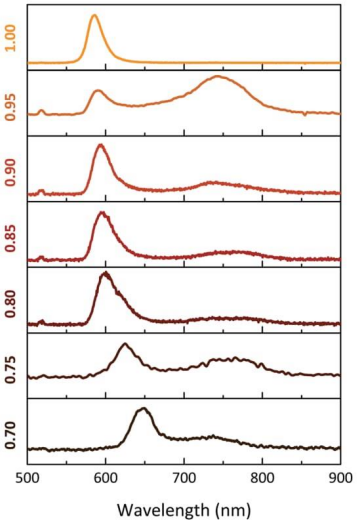

Fig. 3 Photoluminescence spectra of $Cs_{0.15}FA_{0.85}Pb(Br_xI_{1-x})_3$. Thin films recorded immediately after turning on the laser. The different colours represent the fraction of bromide ions relative to the total halide content. The peak at 515 nm originates from the excitation source.

the laser is turned on for each composition, while Fig. 4 shows the evolution of the PL spectrum for the $Cs_{0.15}FA_{0.85}Pb(Br_{0.7}I_{0.3})_3$ composition over time. All spectra exhibit an intense luminescence peak associated with the band-to-band recombination, hence blue-shifting for increasing Br content. However, a second weak signal at lower emission energy is present in all mixed halide perovskites.

Interestingly, the photoluminescence peaks of the mixed $Cs_{0.15}FA_{0.85}Pb(Br_{0.7}I_{0.3})_3$ perovskites change over time. The

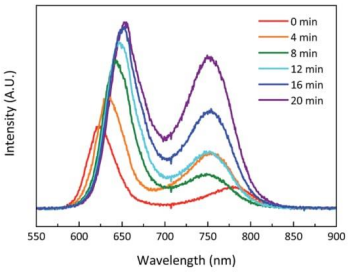

Fig. 4 Evolution of the photoluminescence spectrum over time for a $Cs_{0.15}FA_{0.85}Pb(Br_{0.7}I_{0.3})_3$ perovskite thin film.

speed of the change is dependent on the initial composition of the perovskite material, and also on the precursor batch used to deposit the thin films. This behaviour has previously been observed and it is due to a photoinduced halide segregation.[29] The lower energy peak stabilizes after few minutes, while the higher energy component continues to shift towards longer wavelengths. It has already been shown that the existence of mobile ionic species in perovskite type materials is possible,[36] hence most likely under illumination bromide ions slowly migrate to feed an iodide-rich phase. The growing luminescence feature at about 750 nm probably originates from the forming iodide-rich minority phase, while the increasing intensity of the red-shifting peak at higher energy could be due to the increasing quantum yield of the majority phase as it is losing its bromide content.[37]

While it has been shown that FA^+ and Cs^+ ions do help the stability of the mixed halide perovskite extending their miscibility to more bromide-rich compositions, the results we present here indicate that these materials are still not completely stable, which is one of the reasons for the limited efficiencies observed in the recent reports of 2 terminal tandem cells.[23,24] In spite of this, the quality of the devices is rather good as can be seen from the high efficiencies obtained. This clearly shows the potential of mixed I^-/Br^- systems and encourages further research on the effect of ionic exchange/migration on the perovskite structure under illumination.

Conclusions

A reproducible method to prepare efficient wide band gap perovskite solar cells is presented. Benefiting from the stabilizing effect of Cs^+ and FA^+ cations, the devices outperform previously reported solar cells based on mixed I^-/Br^- perovskite absorbers to achieve similar wide band gaps. The champion device was obtained using the $Cs_{0.15}FA_{0.85}Pb(Br_{0.7}I_{0.3})$ perovskite, with a PCE of 11.5%. The high FF of about 80% and the close to optimal J_{sc} values enable this material to be used as a complementary absorber to $MAPbI_3$. However, photoluminescence measurements showed that the photoinduced halide segregation is present even in these perovskite stoichiometries, limiting the maximum achievable V_{oc}. These results encourage further research on the effect of different ions on the stabilization of the perovskite structure, in particular for the development of all-perovskite monolithic tandem solar cells.

Acknowledgements

We acknowledge financial support from the European Union H2020 project INFORM (grant 675867), the Spanish Ministry of Economy and Competitiveness (MINECO) *via* the Unidad de Excelencia María de Maeztu MDM-2015-0538, MAT2014-55200 and PCIN-2015-255 and the Generalitat Valenciana (Prometeo/2012/053). M. S. and C. M. thank the MINECO for their post-doctoral (JdC) and pre-doctoral grants, respectively. J. A. thanks the Spanish Ministry of Education, Culture and Sport for his pre-doctoral grant.

Notes and references

1 T. Salim, S. Sun, N. Mathews, M. Duchamp, C. Boothroyd, G. Xing, T. C. Sumbce and Y. M. Lam, *Energy Environ. Sci.*, 2014, **7**, 399.

2 C. Wehrenfennig, M. Liu, H. J. Snaith, M. B. Johnston and L. M. Herz, *J. Phys. Chem. Lett.*, 2014, **5**, 1300–1306.

3 A. M. A. Leguy, P. Azarhoosh, M. I. Alonso, M. Campoy-Quiles, O. J. Weber, J. Yao, D. Bryant, M. T. Weller, J. Nelson, A. Walsh, M. van Schilfgaarde and P. R. F. Barnes, *Nanoscale*, 2016, **8**, 6317.

4 A. Miyata, A. Mitioglu, P. Plochocka, O. Portugall, J. T.-W. Wang, S. D. Stranks, H. J. Snaith and R. J. Nicholas, *Nat. Phys.*, 2015, **11**, 582–587.

5 S. D. Stranks, G. E. Eperon, G. Grancini, C. Menelaou, M. J. P. Alcocer, T. Leijtens, L. M. Herz, A. Petrozza and H. J. Snaith, *Science*, 2013, **342**, 341–344.

6 A. Kojima, K. Teshima, Y. Shirai and T. Miyasaka, *J. Am. Chem. Soc.*, 2009, **131**, 6050–6051.

7 M. A. Green, K. Emery, Y. Hishikawa, W. Warta and E. D. Dunlop, *Prog. Photovoltaics*, 2016, **24**, 905–913.

8 P. Docampo, J. M. Ball, M. Darwich, G. E. Eperon and H. J. Snaith, *Nat. Commun.*, 2013, **4**, 2761.

9 Y. Wu, A. Islam, X. Yang, C. Qin, J. Liu, K. Zhang, W. Penga and L. Han, *Energy Environ. Sci.*, 2014, **7**, 2934.

10 W. Nie, H. Tsai, R. Asadpour, J.-C. Blancon, A. J. Neukirch, G. Gupta, J. J. Crochet, M. Chhowalla, S. Tretiak, M. A. Alam, H.-L. Wang and A. D. Mohite, *Science*, 2015, **347**, 522–525.

11 J.-H. Im, I.-H. Jang, N. Pellet, M. Grätzel and N.-G. Park, *Nat. Nanotechnol.*, 2014, **9**, 927–932.

12 S. Colella, E. Mosconi, P. Fedeli, A. Listorti, F. Gazza, F. Orlandi, P. Ferro, T. Besagni, A. Rizzo, G. Calestani, G. Gigli, F. De Angelis and R. Mosca, *Chem. Mater.*, 2013, **25**, 4613–4618.

13 W. Zhang, M. Saliba, D. T. Moore, S. K. Pathak, M. T. Hörantner, T. Stergiopoulos, S. D. Stranks, G. E. Eperon, J. A. Alexander-Webber, A. Abate, A. Sadhanala, S. Yao, Y. Chen, R. H. Friend, L. A. Estroff, U. Wiesner and H. J. Snaith, *Nat. Commun.*, 2015, **6**, 6142.

14 D. Forgács, M. Sessolo and H. J. Bolink, *J. Mater. Chem. A*, 2015, **3**, 14121.

15 D. T. Moore, H. Sai, K. W. Tan, D.-M. Smilgies, W. Zhang, H. J. Snaith, U. Wiesner and L. A. Estroff, *J. Am. Chem. Soc.*, 2015, **137**, 2350–2358.

16 M. M. Lee, J. Teuscher, T. Miyasaka, T. N. Murakami and H. J. Snaith, *Science*, 2012, **338**, 643.

17 J. H. Heo, H. J. Han, D. Kim, T. K. Ahn and S. H. Im, *Energy Environ. Sci.*, 2015, **8**, 1602–1608.

18 J. B. Patel, R. L. Milot, A. D. Wright, L. M. Herz and M. B. Johnston, *J. Phys. Chem. Lett.*, 2016, **7**, 96–102.

19 C.-W. Chen, H.-W. Kang, S.-Y. Hsiao, P.-F. Yang, K.-M. Chiang and H.-W. Lin, *Adv. Mater.*, 2014, **26**, 6647–6652.

20 K. Yan, M. Long, T. Zhang, Z. Wei, H. Chen, S. Yang and J. Xu, *J. Am. Chem. Soc.*, 2015, **137**, 4460–4468.

21 W. Jérémie, L. Barraud, A. Walter, M. Bräuninger, F. Sahli, D. Sacchetto, N. Tétreault, B. P. Salomon, S.-J. Moon, C. Allebé, M. Despeisse, S. Nicolay, S. De Wolf, B. Niesen and C. Ballif, *ACS Energy Lett.*, 2016, **1**, 474–480.

22 B. Chen, Y. Bai, Z. Yu, T. Li, X. Zheng, Q. Dong, L. Shen, M. Boccard, A. Gruverman, Z. Holmanand and J. Huang, *Adv. Energy Mater.*, 2016, **6**, 1601128.

23 G. E. Eperon, T. Leijtens, K. A. Bush, T. Green, J. T.-W. Wang, D. P. McMeekin, G. Volonakis, R. L. Milot, D. J. Slotcavage, R. Beslile, J. B. Patel, E. S. Parrott, R. J. Sutton, W. Ma, F. Moghadam, B. Conings, A. Babayigit, H.-G. Boyen, F. Giustino, L. M. Herz, M. B. Johnston, M. D. McGehee and H. J. Snaith, *Science*, 2016, **354**, 861–865.

24 D. Forgács, L. Gil-Escrig, D. Pérez-Del-Rey, C. Momblona, J. Werner, B. Niesen, C. Ballif, M. Sessolo and H. J. Bolink, *Adv. Energy Mater.*, 2016, DOI: 10.1002/aenm.201602121.

25 S. A. Kulkarni, T. Baikie, P. P. Boix, N. Yantara, N. Mathews and S. Mhaisalkar, *J. Mater. Chem. A*, 2014, **2**, 9221.

26 Y. Zhou, M. Yang, O. S. Game, W. Wu, J. Kwun, M. A. Strauss, J. Huang, Y. Yan, K. Zhu and N. P. Padture, *ACS Appl. Mater. Interfaces*, 2016, **8**, 2232–2237.

27 R. E. Beal, D. J. Slotcavage, T. Leijtens, A. R. Bowring, R. A. Belisle, W. H. Nguyen, G. F. Burkhard, E. T. Hoke and M. D. McGehee, *J. Phys. Chem. Lett.*, 2016, **7**, 746–751.

28 M. Jaysankar, W. Qiu, J. Bastos, J. G. Tait, M. Debucquoy, U. W. Paetzold, D. Cheynsand and J. Poortmans, *J. Mater. Chem. A*, 2016, **4**, 10524–10531.

29 E. T. Hoke, D. J. Slotcavage, E. R. Dohner, A. R. Bowring, H. I. Karunadasa and M. D. McGehee, *Chem. Sci.*, 2015, **6**, 613.

30 D. J. Slotcavage, H. I. Karunadasa and M. D. McGehee, *ACS Energy Lett.*, 2016, **1**, 1199–1205.

31 M. Saliba, T. Matsui, J.-Y. Seo, K. Domanski, J.-P. Correa-Baena, M. K. Nazeeruddin, S. M. Zakeeruddin, W. Tress, A. Abate, A. Hagfeldt and M. Grätzel, *Energy Environ. Sci.*, 2016, **9**, 1989.

32 D. P. McMeekin, G. Sadoughi, W. Rehman, G. E. Eperon, M. Saliba, M. T. Hörantner, A. Haghighirad, N. Sakai, L. Korte, B. Rech, M. B. Johnston, L. M. Herz and H. J. Snaith, *Science*, 2016, **351**, 151–155.

33 L. Gil-Escrig, C. Momblona, M. Sessolo and H. J. Bolink, *J. Mater. Chem. A*, 2016, **4**, 3667.

34 C. Momblona, L. Gil-Escrig, E. Bandiello, E. M. Hutter, K. Lederer, M. Sessolo, J. Blochwitz-Nimoth and H. J. Bolink, *Energy Environ. Sci.*, 2016, **9**, 3456.

35 H.-S. Kim and N.-G. Park, *J. Phys. Chem. Lett.*, 2014, **5**, 2927–2934.

36 E. Bandiello, J. Ávila, L. Gil-Escrig, E. Tekelenburg, M. Sessolo and H. J. Bolink, *J. Mater. Chem. A*, 2016, **4**, 18614–18620.

37 S. J. Yoon, S. Draguta, J. S. Manser, O. Sharia, W. F. Schneider, M. Kuno and P. V. Kamat, *ACS Energy Lett.*, 2016, **1**, 290–296.

6 Perovskite-perovskite tandem cells

As discussed in previous chapters, the development of perovskite/perovskite tandem photovoltaics holds enormous market potential, however it is hindered by several intrinsic technical challenges. Besides the need to develop and optimize new perovskite materials that enable efficient complementary light harvesting properties, there are difficulties arising from processing multilayer architectures from solutions. There is an additional challenge that has to be overcome in monolithic tandem cells, which is the preparation of efficient charge recombination layers (CRL) between the active materials. CRLs have to be highly conductive and transparent in order to eliminate possible losses in power generation, and should be compatible with multi-layer processing. Well-established systems for the preparation of CRLs are doped organic semiconductors that are widely used in organic light emitting diodes and organic photovoltaic devices. Using vacuum deposition methods, the process becomes intrinsically additive as the deposition is virtually substrate-independent.

As we have already demonstrated the preparation of highly efficient wide band gap perovskite solar cells, our next goal was to incorporate them in a tandem architecture. In this part of the thesis, we have created an n-i-p perovskite/perovskite tandem solar cell, using a multilayer CRL employing intrinsic and doped organic semiconductors. On top of the $Cs_{0.15}FA_{0.85}Pb(Br_{0.7}I_{0.3})_3$ layer, we deposited a CRL, using N4,N4,N4″,N4″-tetra([1,1′-biphenyl]-4-yl)-[1,1′:4′,1″-terphenyl]-4,4″-diamine (TaTm) as the p-type HTL, fullerene C60 as an n-type ETL, and 2,2′-(perfluoronaphthalene-2,6-diylidene) dimalononitrile (F_6-TCNNQ) as the p-type dopant and N1,N4-bis(tri-p-tolylphosphoranylidene) benzene-1,4-diamine (PhIm) as the n-type dopant respectively. The device was finished with a vacuum deposited MAPI/TaTm/doped TaTm/Au multi-layer.

The prepared tandem perovskite solar cells exhibited a V_{oc} which is close to the sum of the photovoltage of the single sub cells, indicating an efficient CRL. In this layout, we have achieved a maximum efficiency of 18.1% that is very close to that of the single MAPI cell. The main limitation of this value stems from the photo-instability of the wide band gap absorber, which results in a limited voltage contribution. Also, this tandem device could be further improved by tuning the band gap of both absorbers to more optimal values (towards the infrared). Regardless of these shortcomings, we have shown a viable strategy to fabricate perovskite/perovskite tandem solar cells, which might even be used for triple junction devices with silicon or CIGS cells.

ADVANCED ENERGY MATERIALS
www.advenergymat.de

Efficient Monolithic Perovskite/Perovskite Tandem Solar Cells

Dávid Forgács, Lidón Gil-Escrig, Daniel Pérez-Del-Rey, Cristina Momblona, Jérémie Werner, Bjoern Niesen, Christophe Ballif, Michele Sessolo, and Henk J. Bolink*

Organic–inorganic (hybrid) perovskites are at the forefront of emerging photovoltaic materials, thanks to their fast rising and constantly improving power conversion efficiencies (PCEs), which are now exceeding 22%.[1–6] While the development of novel absorber materials is likely to further enhance the performances of perovskite solar cells, the use of novel architectures such as tandem cells is a proven successful strategy to overcome the Shockley–Queisser limit of single junction devices. Hybrid perovskites are quite unique, being efficient semiconductors whose bandgap can be readily tuned over a wide range, allowing light absorption from near-infrared to visible wavelengths.[7,8] For this reason, they are being investigated as top cells in combination with a variety of narrow bandgap solar cells,[9–12] in particular with silicon[7,13–17] and copper indium gallium selenide.[15,18–20] The challenges associated with the advance of perovskite tandem solar cells include the development of charge recombination layers (CRLs) between the two subcells with low ohmic losses and of deposition processes that are compatible with the underline photovoltaic cells. Hence, most of the reported tandem devices consist in mechanically stacked semitransparent cells (4-terminal cells), while only few recent examples have demonstrated the fabrication of monolithic, 2-terminal photovoltaic devices.[21–25] An alternative strategy is the development of perovskite–perovskite tandem devices, which could profit from the simple bandgap tuning of perovskite absorbers and from the use of inexpensive precursor materials. The first example of perovskite–perovskite tandem used two analogue subcells with the same absorbing material, methylammonium lead iodide ($MAPbI_3$), which were connected by lamination with a 2 μm thick, doped hole transport layer (HTL).[26] Despite the demonstration of an open-circuit voltage (V_{oc}) as high as 2.2 V (the exact sum of the photovoltage produced by the two subcells), the PCE was limited by the use of the same absorber, which in turn strongly reduced the overall attainable current density. In another work, a monolithic perovskite–perovskite tandem device was fully solution processed using a multilayer organic CRL, which is challenging due to the requirement of solvent orthogonality during processing of each of the layers.[27] Also in this case the two subcells used an identical perovskite absorber, $MAPbI_3$, hence limiting the overall PCE. In order to prepare efficient tandem structures, the development of complementary, narrow bandgap perovskite materials is also being pursued.[28] Recently, Yang et al. presented the narrow bandgap (1.33 eV) $MA_{0.5}FA_{0.5}Pb_{0.75}Sn_{0.25}I_3$ perovskite, which could lead to single junction cells with a PCE of 14.19%.[29] They also fabricated a 4-terminal tandem using the narrow bandgap mixed perovskite in combination with a semitransparent $MAPbI_3$ cell (used as the wide bandgap material), achieving a PCE of about 19%. In general, the deposition of the CRL remains challenging, since it has to fulfill the requirements of high transparency, high conductivity, and at the same time the deposition process must be compatible with the underlying perovskite and organic transport layers. A valuable alternative in the preparation of tandem solar cells is the use of doped organic semiconductors, which have been widely studied for tandem organic light-emitting diodes and small molecular weight organic photovoltaics.[30–32] In these materials the conductivity can be tuned over several orders of magnitude by simply varying the dopant concentration, yet maintaining a high optical transmittance.[33] Importantly, organic semiconductors can be processed by simple vacuum deposition techniques which are intrinsically additive, meaning that multilayer devices can be built without chemical modifications of the underlying layers or the use of orthogonal solvents.[34,35] The low fabrication temperature makes vacuum deposition compatible with any underlying active material and in general with a wide range of substrates, including flexible and textiles. Also, vacuum deposited films are able to conform with the substrate morphology, an important feature in the preparation of tandem devices on textured silicon cells.[24]

In this work we present efficient monolithic tandem solar cells based on two perovskite absorbers with different and complementary bandgaps. For the front subcell, a wide bandgap perovskite with composition $Cs_{0.15}FA_{0.85}Pb(I_{0.3}Br_{0.7})_3$ was used as the absorber.[28] The rear subcell used the well-known narrow bandgap perovskite $MAPbI_3$ as the absorber. The wide bandgap perovskite is solution processed yet the remaining materials needed to construct the tandem devices are all deposited using thermal evaporation. By employing doped organic semiconductors, an efficient extraction and transport of the photogenerated

D. Forgács, L. Gil-Escrig, D. Pérez-Del-Rey, C. Momblona, Dr. M. Sessolo, Dr. H. J. Bolink
Instituto de Ciencia Molecular
Universidad de Valencia
C/J. Beltrán 2, 46980 Paterna, Spain
E-mail: michele.sessolo@uv.es
J. Werner, Dr. B. Niesen, Prof. C. Ballif
Ecole Polytechnique Fédérale de Lausanne (EPFL)
Institute of Microengineering (IMT)
Photovoltaics and Thin-Film Electronics Laboratory
Rue de la Maladière 71b, 2002 Neuchâtel, Switzerland
Dr. B. Niesen, Prof. C. Ballif
CSEM
PV-Center
Rue Jaquet-Droz 1, 2002 Neuchâtel, Switzerland

DOI: 10.1002/aenm.201602121

charge carriers is ensured, while carrier recombination at the perovskite interfaces is prohibited by using intrinsic and selective charge transport layers. Despite the nonideal combination of bandgaps in the two subcells, we demonstrate perovskite–perovskite tandem cells delivering an average PCE of 15%, and a record efficiency of 18%. This work demonstrates the potential of vacuum deposited multilayer structures in overcoming the efficiency of state of the art perovskite solar cells.

Thin films of the mixed perovskite $Cs_{0.15}FA_{0.85}Pb(I_{0.3}Br_{0.7})_3$ have been prepared from solution following a recently published protocol (details in the Supporting Information).[28] This particular composition has been reported to lead to a semiconducting perovskite with an optical bandgap of ≈2 eV, which would maximize the efficiency of a tandem device when the absorber of the second subcell is $MAPbI_3$, with a bandgap of 1.55 eV.[36]

$MAPbI_3$ layers have been prepared by dual source vapor deposition in a high vacuum chamber using a published procedure (details of the deposition can be found in the Supporting Information).[37] The optical absorption spectra and grazing incidence X-ray diffraction (GIXRD) patterns of both perovskite thin films are depicted in **Figure 1**a,b, respectively, and essentially confirm the formation of highly absorbing polycrystalline perovskite thin films.[28,37] Small molecular weight, sublimable organic semiconductors were employed to form selective charge transporting layers adjacent to the perovskite absorbers in the tandem structure. The optimization of these materials and their dopants, in combination with the $MAPbI_3$ perovskite absorber for single junction solar cells, was recently described by Momblona et al.[38] In Figure 1c, the chemical structures of the charge transport molecules and of their dopants used in this work are reported. As the hole transport material, we have used the N4,N4,N4″,N4″-tetra([1,1′-biphenyl]-4-yl)-[1,1′:4′,1″-terphenyl]-4,4″-diamine (TaTm), whose conductivity can be tuned by two orders of magnitude by doping it with 2,2′-(perfluoronaphthalene-2,6-diylidene) dimalononitrile (F_6-TCNNQ).[38] The fullerene C_{60} was selected as the electron transport material as it has been used as an efficient electron acceptor in perovskite solar cells.[39] Efficient modulation of the C_{60} conductivity can be obtained by codeposition with N1,N4-bis(tri-p-tolylphosphoranylidene) benzene-1,4-diamine (PhIm).[38] The fullerene derivative indene-C_{60}-propionic acid hexyl ester (IPH) was used as a solution-processable interlayer on top of TiO_2, in order to reduce surface recombination and enhance photovoltage (Figure S1, Supporting Information).[28,40] Hence, only the TiO_2 electron transport layer (ETL) and the wide bandgap perovskite absorber are solution processed in this monolithic tandem architecture. This method was selected as mixed ion perovskite preparation using simultaneous sublimation of multiple precursor compounds is rather complicated and still under development. Prior to the integration into monolithic tandem devices, the subcell absorbers were evaluated in single-junction solar cells. The single junction $MAPbI_3$ cells were fully vacuum deposited onto ITO-coated glass slides, using an n–i–p architecture (ETL is deposited on the transparent conductor), as shown in **Figure 2**a. Briefly, a 40 nm thick film of C_{60}:PhIm (60 wt%) (C_{60} doped with PhIm at 60% in weight) is deposited onto the ITO, followed by a 10 nm thick intrinsic C_{60} ETL, which selectively transports electrons confining the holes in the active layer. Subsequently, the $MAPbI_3$ perovskite absorber (500 nm) is deposited by dual source vapor deposition without any thermal treatment. Then, a thin intrinsic TaTm hole transport layer (HTL, 10 nm) is deposited on the perovskite followed by a 40 nm thick TaTm:F_6-TCNNQ

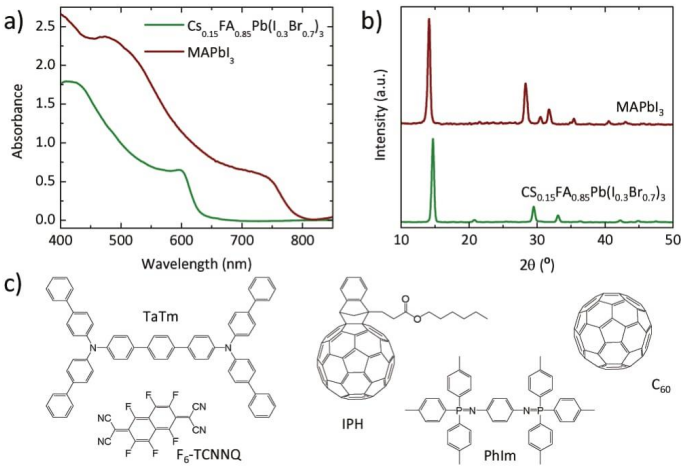

Figure 1. Characterization of perovskite thin films. a) Absorption spectra of $Cs_{0.15}FA_{0.85}Pb(I_{0.3}Br_{0.7})_3$ (300 nm) and $MAPbI_3$ (500 nm). b) GIXRD patterns for the same perovskite films. c) Chemical structures of the organic semiconductors and dopants used as charge transport layers in the photovoltaic devices.

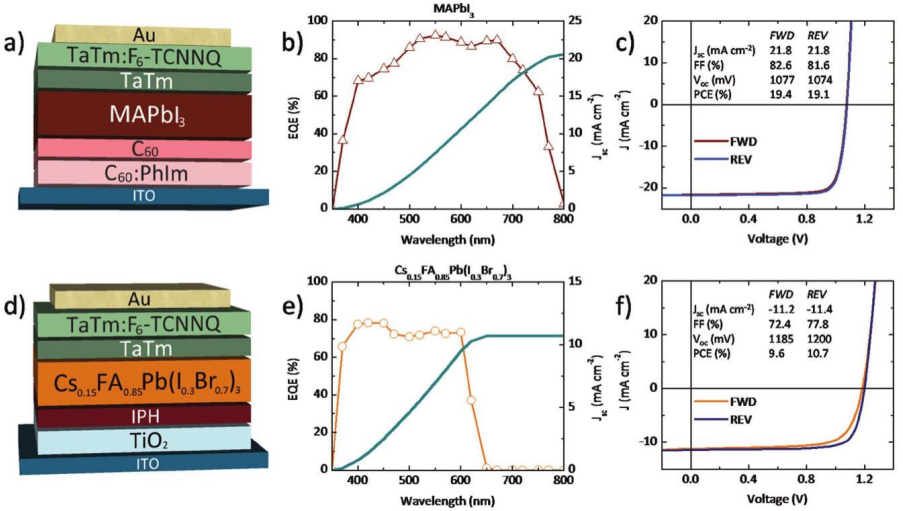

Figure 2. Characterization of single junction perovskite solar cells: a,d) device structures, b,e) external quantum efficiencies (EQE, left), with corresponding integrated photocurrent with the AM1.5G solar spectrum (right axis), and c,f) *J–V* curves under 100 mW cm^{-2} illumination in forward (FWD) and reverse (REV) bias, for a fully vacuum deposited n–i–p $MAPbI_3$ cell and for the wide bandgap perovskite device, respectively.

(11 wt%) film. The device is finished with the deposition of a gold electrode.

Single junction cells based on the wide bandgap absorber $Cs_{0.15}FA_{0.85}Pb(I_{0.3}Br_{0.7})_3$ were built using an n–i–p architecture as well (Figure 2d, details in the Supporting Information). In this case, the ITO was coated with an 80 nm thick TiO_2 ETL prepared by spin-coating of NPs suspensions (diameter 15–20 nm) and annealed at 200 °C for 30 min. Afterward, a thin (10–20 nm) layer of IPH was solution processed from its chlorobenzene solution and annealed at 70 °C for 10 min. The mixed perovskite was spin-coated on top of the IPH from a dimethyl sulfoxide solution, and annealed at 70 °C for 30 s and at 100 °C for 1 h. Besides a partial removal of the IPH during the deposition of the perovskite films, the presence of IPH had a beneficial effect on the device photovoltage (Figure S1, Supporting Information), most likely due to a diminished carrier recombination. Following the perovskite layer formation, a thin (10 nm) intrinsic TaTm HTL and a 40 nm thick TaTm:F_6-TCNNQ (11 wt%) layer were vacuum deposited on the perovskite and capped with a gold electrode.

The devices were first characterized measuring their external quantum efficiency (EQE) as a function of the incident light wavelength (Figure 2b). The optimized $MAPbI_3$ cells, as recently described,[38] show a very high photocurrent response over the whole visible spectrum, with EQE as high as 90% between 500 and 700 nm. This is a consequence of the high absorbance of the perovskite films and of the very low optical absorption characteristic of the doped C60:PhIm film (Figure S2, Supporting Information) used at the front contact. Such high EQE results in a short-circuit current density (J_{sc}) exceeding 20 mA cm^{-2}, in accordance with previous results on analogous devices. The current density versus voltage (*J–V*) characteristics under 100 mW cm^{-2} illumination for the best cell measured during this set of experiments is reported in Figure 2c. The curve shows a very high fill factor (FF, >80%) and V_{oc}, resulting from the efficient extraction of the charge carriers due to the doped interfaces and to a low charge recombination. The solar cell shows negligible *J–V* hysteresis with a PCE exceeding 19%, both when measured in forward (FWD, from J_{sc} to V_{oc}) and in reverse (REV, from V_{oc} to J_{sc}) bias.

The average values of the photovoltaic parameters with their standard deviation (SD), calculated on 16 $MAPbI_3$ cells and measured under forward as well as in reverse bias, are reported in **Table 1**. We obtained an average PCE of 17.3% and 17.4% in forward and reverse bias, respectively, with a SD of less than 2% and the small cell-to-cell variability mainly determined by the photocurrent and FF. The obtained wide bandgap solar cells show a high photocurrent response over the whole visible spectrum, with EQE of 70 to 80% until 600 nm, where the spectral response drops since it coincides with the perovskite bandgap (Figure 2e). The lower spectral EQE (when compared to the $MAPbI_3$ cells) is likely due to the relatively thin absorber used, which is limited by the solubility of the CsBr precursor in dimethyl sulfoxide. The EQE results in a J_{sc} exceeding 10 mA cm^{-2} on average (Table 1). The *J–V* characteristics under 100 mW cm^{-2} illumination for the best cell measured during this set of experiments is reported in Figure 2f. Similar to most metal oxide containing perovskite solar cells, we observed a small but noticeable current hysteresis, with a reduced FF in the forward bias scan. For the record cell, this translates into

Table 1. Performance overview for single-junction perovskite solar cells obtained in forward (FWD) and reverse (REV) bias. The average (Avg.) values with their standard deviation (SD) are reported and compared with their maximum (Max).

	$MAPbI_3$					
	FWD			REV		
	Avg.	SD	Max	Avg.	SD	Max
V_{oc} [mV]	1059	±16	1079	1074	±22	1103
J_{sc} [mA cm^{-2}]	−20.64	±0.75	−21.89	−20.54	±0.79	−21.89
FF [%]	78.8	±3.4	82.6	79.0	±2.5	81.6
PCE [%]	17.3	±1.4	19.4	17.4	±1.1	19.1
	$Cs_{0.15}FA_{0.85}Pb(I_{0.3}Br_{0.7})_3$					
	FWD			REV		
	Avg.	SD	Max	Avg.	SD	Max
V_{oc} [mV]	1159	±32	1194	1167	±42	1215
J_{sc} [mA cm^{-2}]	−10.42	±0.59	−11.22	−10.24	±0.57	−11.41
FF [%]	68.5	±3.3	72.4	75.6	±5.1	81.2
PCE [%]	8.3	±0.9	9.6	9.0	±1.0	10.7

a difference in PCE from 10.7% in reverse bias to 9.6% when the solar cell is forward biased. V_{oc} values as high as 1.2 V have been recorded, the average lying at about 1160 mV, which is in line with those presented previously, but still low taking into account the bandgap of the absorber (≈2 eV).[28] We obtained an average PCE of 8.3% and 9.0% in forward and reverse bias, respectively, with the cell-to-cell variability mainly determined by V_{oc}, and the *J*–*V* hysteresis being correlated with the variation of the FF.

The fabrication of the monolithic perovskite–perovskite tandem starts with the processing of the wide bandgap $Cs_{0.15}FA_{0.85}Pb(I_{0.3}Br_{0.7})_3$ cell as described before, which instead of being finished with the gold electrode, is completed by direct deposition of the full $MAPbI_3$ stack, as represented in **Figure 3**a.

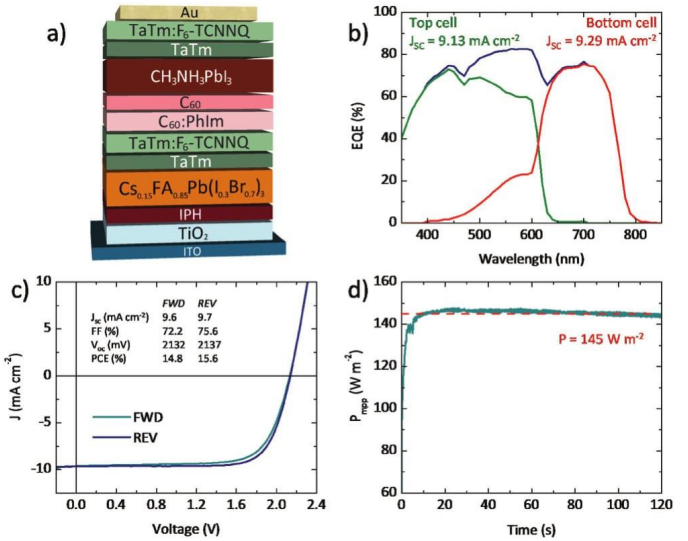

Figure 3. Characterization of monolithic perovskite-perovskite solar cells: a) device structure, b) external quantum efficiency (EQE, left), with highlighted the measured photocurrent density for each subcell. c) *J*–*V* curves under 100 mW cm^{-2} illumination in forward (FWD) and reverse (REV) bias, and d) steady power output under maximum power point tracking for the same device.

In this way the layer stack in between the two different perovskite absorbers consist of a p-doped HTL and an n-doped ETL, TaTm:F_6-TCNNQ (40 nm)/C_{60}:PhIm (40 nm), that is known to function efficiently as a charge recombination layer. Vacuum deposition allows to circumvent the challenges associated with the monolithic integration of two subcells, since no damage of the underlying layer can occur and no thermal treatment is needed. The EQE spectra for a tandem device are reported in Figure 3b, where the contribution for each subcell with corresponding current density is highlighted. The wide bandgap cell delivers a current density of 9.13 mA cm^{-2}, while the bottom $MAPbI_3$ cell produces a slightly higher current of 9.29 mA cm^{-2}, which brings the tandem close to the current-matched situation.

The *J–V* characteristics show only small hysteresis (lower when compared to the single junction wide bandgap cell), with a FF of 72.2% and 75.6% when the cell is measured in forward and reverse bias, respectively (Figure 3c). Importantly, a V_{oc} as high as 2132 and 2137 mV was observed in forward and reverse bias, respectively. From the average photovoltaic parameters (estimated from 48 tandem cells, **Table 2**), one can see how the average V_{oc} obtained from the tandem devices in both reverse and forward bias is very close to the sum of the average photovoltage of each subcell (Table 1), which highlights the high quality of the CRL and in general of the device architecture used. The average PCE for the tandem cell is 14.8% in forward and 15.6% in reverse bias, again due to the slightly higher FF observed when measuring the cells from open to short-circuit. Interestingly, the steady power output measured under maximum power point tracking shows a steady-state efficiency of 14.5% (145 W m^{-2}) after 2 min of illumination, within the average PCE observed (Table 2). The top performing device exhibited a PCE of 18.1% in reverse bias, which is important considering that the theoretical maximum PCE for this bandgap pair lies in the 20%–25% range.[36] In the best performing device, the V_{oc} approaches 2.3 V, which is the exact sum of the record V_{oc} obtained for the 2 subcells. To address the stability of the materials and the device architecture, encapsulated devices were kept in ambient conditions and measured for several days after preparation. The device performance of the cells kept in the dark during several days was, after a short period of illumination, almost identical to that observed on the first day. These preliminary data indicate that these devices have a promising stability (Figure S3, Supporting Information), maintaining more than 98% of the original PCE after 3 d.

Table 2. Performance overview for monolithic perovskite–perovskite solar cells obtained in forward (FWD) and reverse (REV) bias. The average (Avg.) values with their standard deviation (SD) obtained from 48 cells, and the photovoltaic parameters for the best performing device are reported.

	FWD		REV		Record cell	
	Avg.	SD	Avg.	SD	FWD	REV
V_{oc} [mV]	2206	±48	2192	±61	2281	2294
J_{sc} [mA cm^{-2}]	−9.48	±0.44	−9.35	±0.43	−10.01	−9.83
FF [%]	70.7	±4.0	74.3	±5.2	76.1	80.3
PCE [%]	14.8	±1.5	15.3	±1.5	17.4	18.1

The performances of perovskite/perovskite tandem devices presented here are extremely promising and were enabled by the use of doped and intrinsic small-molecule organic semiconductors. Furthermore, these results validate vacuum deposition as a relevant tool in the development of efficient perovskite solar cells, which is important considering that vacuum coating techniques are the standard in the semiconductor industry. Notably, by choosing more appropriate complementary bandgaps, for example, by exchanging the $MAPbI_3$ absorber for a narrower bandgap perovskite, efficiencies in excess of those demonstrated for single junction perovskite solar cells are achievable.

Supporting Information

Supporting Information is available from the Wiley Online Library or from the author.

Acknowledgements

The authors are grateful to Novaled GmbH, in particular to Jan Blochwitz-Nimoth for the supply of the organic charge transport materials and dopandts. The authors further acknowledge financial support from the European Union H2020 project INFORM (Grant No. 675867), the Spanish Ministry of Economy and Competitiveness (MINECO) via the Unidad de Excelencia María de Maeztu MDM-2015-0538, MAT2014-55200-R, and PCIN-2015-255 and the Generalitat Valenciana (Prometeo/2016/135). C.M. and M.S. thank the MINECO for their pre- and post-doctoral (JdC) contracts. The project comprising this work is evaluated by the Swiss National Science Foundation and funded by the Nano-Tera.ch project "Synergy" and by the PNR 70 project "PV2050" with financing from the Swiss National Science Foundation and by the Swiss Federal Office of Energy, under Grant No. SI/501072-01.

Received: September 22, 2016
Revised: October 31, 2016
Published online:

[1] W. S. Yang, J. H. Noh, N. J. Jeon, Y. C. Kim, S. Ryu, J. Seo, S. I. Seok, *Science* **2015**, *348*, 1234.
[2] D. Bi, W. Tress, M. I. Dar, P. Gao, J. Luo, C. Renevier, K. Schenk, A. Abate, F. Giordano, J.-P. Correa Baena, J.-D. Decoppet, S. M. Zakeeruddin, M. K. Nazeeruddin, M. Grätzel, A. Hagfeldt, *Sci. Adv.* **2016**, *2*, e1501170.
[3] M. Saliba, T. Matsui, J.-Y. Seo, K. Domanski, J.-P. Correa-Baena, M. K. Nazeeruddin, S. M. Zakeeruddin, W. Tress, A. Abate, A. Hagfeldt, M. Gratzel, *Energy Environ. Sci.* **2016**, *9*, 1989.
[4] T. Jesper Jacobsson, J.-P. Correa-Baena, M. Pazoki, M. Saliba, K. Schenk, M. Gratzel, A. Hagfeldt, *Energy Environ. Sci.* **2016**, *9*, 1706.
[5] X. Li, D. Bi, C. Yi, J.-D. Décoppet, J. Luo, S. M. Zakeeruddin, A. Hagfeldt, M. Grätzel, *Science* **2016**, *353*, 58.
[6] M. A. Green, K. Emery, Y. Hishikawa, W. Warta, E. D. Dunlop, *Prog. Photovolt: Res. Appl.* **2016**, *24*, 905.
[7] C. D. Bailie, M. D. McGehee, *MRS Bull.* **2015**, *40*, 681.
[8] T. Todorov, O. Gunawan, S. Guha, *Mol. Syst. Des. Eng.* **2016**, DOI: 10.1039/C6ME00041J.
[9] T. Todorov, T. Gershon, O. Gunawan, C. Sturdevant, S. Guha, *Appl. Phys. Lett.* **2014**, *105*, 173902.
[10] C.-C. Chen, S.-H. Bae, W.-H. Chang, Z. Hong, G. Li, Q. Chen, H. Zhou, Y. Yang, *Mater. Horiz.* **2015**, *2*, 203.

[11] Y. Liu, L. A. Renna, M. Bag, Z. A. Page, P. Kim, J. Choi, T. Emrick, D. Venkataraman, T. P. Russell, *ACS Appl. Mater. Interfaces* **2016**, *8*, 7070.
[12] J. Liu, S. Lu, L. Zhu, X. Li, W. C. H. Choy, *Nanoscale* **2016**, *8*, 3638.
[13] P. Loper, S.-J. Moon, S. Martin de Nicolas, B. Niesen, M. Ledinsky, S. Nicolay, J. Bailat, J.-H. Yum, S. De Wolf, C. Ballif, *Phys. Chem. Chem. Phys.* **2015**, *17*, 1619.
[14] F. Lang, M. A. Gluba, S. Albrecht, J. Rappich, L. Korte, B. Rech, N. H. Nickel, *J. Phys. Chem. Lett.* **2015**, *6*, 2745.
[15] C. D. Bailie, M. G. Christoforo, J. P. Mailoa, A. R. Bowring, E. L. Unger, W. H. Nguyen, J. Burschka, N. Pellet, J. Z. Lee, M. Gratzel, R. Noufi, T. Buonassisi, A. Salleo, M. D. McGehee, *Energy Environ. Sci.* **2015**, *8*, 956.
[16] K. A. Bush, C. D. Bailie, Y. Chen, A. R. Bowring, W. Wang, W. Ma, T. Leijtens, F. Moghadam, M. D. McGehee, *Adv. Mater.* **2016**, *28*, 3937.
[17] B. Chen, Y. Bai, Z. Yu, T. Li, X. Zheng, Q. Dong, L. Shen, M. Boccard, A. Gruverman, Z. Holman, J. Huang, *Adv. Energy Mater.* **2016**, 1601128.
[18] L. Kranz, A. Abate, T. Feurer, F. Fu, E. Avancini, J. Löckinger, P. Reinhard, S. M. Zakeeruddin, M. Grätzel, S. Buecheler, A. N. Tiwari, *J. Phys. Chem. Lett.* **2015**, *6*, 2676.
[19] F. Fu, T. Feurer, T. Jager, E. Avancini, B. Bissig, S. Yoon, S. Buecheler, A. N. Tiwari, *Nat. Commun.* **2015**, *6*, 8932.
[20] Y. Yang, Q. Chen, Y.-T. Hsieh, T.-B. Song, N. D. Marco, H. Zhou, Y. Yang, *ACS Nano* **2015**, *9*, 7714.
[21] J. P. Mailoa, C. D. Bailie, E. C. Johlin, E. T. Hoke, A. J. Akey, W. H. Nguyen, M. D. McGehee, T. Buonassisi, *Appl. Phys. Lett.* **2015**, *106*, 121105.
[22] T. Todorov, T. Gershon, O. Gunawan, Y. S. Lee, C. Sturdevant, L.-Y. Chang, S. Guha, *Adv. Energy Mater.* **2015**, *5*, 1500799.
[23] J. Werner, C.-H. Weng, A. Walter, L. Fesquet, J. P. Seif, S. De Wolf, B. Niesen, C. Ballif, *J. Phys. Chem. Lett.* **2016**, *7*, 161.
[24] J. Werner, L. Barraud, A. Walter, M. Bräuninger, F. Sahli, D. Sacchetto, N. Tétreault, B. Paviet-Salomon, S.-J. Moon, C. Allebé, M. Despeisse, S. Nicolay, S. De Wolf, B. Niesen, C. Ballif, *ACS Energy Lett.* **2016**, *1*, 474.
[25] S. Albrecht, M. Saliba, J. P. Correa Baena, F. Lang, L. Kegelmann, M. Mews, L. Steier, A. Abate, J. Rappich, L. Korte, R. Schlatmann, M. K. Nazeeruddin, A. Hagfeldt, M. Gratzel, B. Rech, *Energy Environ. Sci.* **2016**, *9*, 81.
[26] J. H. Heo, S. H. Im, *Adv. Mater.* **2016**, *28*, 5121.
[27] F. Jiang, T. Liu, B. Luo, J. Tong, F. Qin, S. Xiong, Z. Li, Y. Zhou, *J. Mater. Chem. A* **2016**, *4*, 1208.
[28] D. P. McMeekin, G. Sadoughi, W. Rehman, G. E. Eperon, M. Saliba, M. T. Hörantner, A. Haghighirad, N. Sakai, L. Korte, B. Rech, M. B. Johnston, L. M. Herz, H. J. Snaith, *Science* **2016**, *351*, 151.
[29] Z. Yang, A. Rajagopal, C.-C. Chueh, S. B. Jo, B. Liu, T. Zhao, A. K. Y. Jen, *Adv. Mater.* **2016**, *28*, 8990.
[30] M. Riede, C. Uhrich, J. Widmer, R. Timmreck, D. Wynands, G. Schwartz, W.-M. Gnehr, D. Hildebrandt, A. Weiss, J. Hwang, S. Sundarraj, P. Erk, M. Pfeiffer, K. Leo, *Adv. Funct. Mater.* **2011**, *21*, 3019.
[31] H. Sasabe, J. Kido, *J. Mater. Chem. C* **2013**, *1*, 1699.
[32] S. Reineke, M. Thomschke, B. Lüssem, K. Leo, *Rev. Mod. Phys.* **2013**, *85*, 1245.
[33] K. Walzer, B. Maennig, M. Pfeiffer, K. Leo, *Chem. Rev.* **2007**, *107*, 1233.
[34] M. Sessolo, C. Momblona, L. Gil-Escrig, H. J. Bolink, *MRS Bull.* **2015**, *40*, 660.
[35] L. K. Ono, M. R. Leyden, S. Wang, Y. Qi, *J. Mater. Chem. A* **2016**, *4*, 6693.
[36] T. J. Coutts, K. A. Emery, J. Scott Ward, *Prog. Photovolt: Res. Appl.* **2002**, *10*, 195.
[37] O. Malinkiewicz, A. Yella, Y. H. Lee, G. M. Espallargas, M. Graetzel, M. K. Nazeeruddin, H. J. Bolink, *Nat. Photonics* **2014**, *8*, 128.
[38] C. Momblona, L. Gil-Escrig, E. Bandiello, E. M. Hutter, M. Sessolo, K. Lederer, J. Blochwitz-Nimoth, H. J. Bolink, *Energy Environ. Sci.* **2016**, *9*, 3456.
[39] P.-W. Liang, C.-C. Chueh, S. T. Williams, A. K. Y. Jen, *Adv. Energy Mater.* **2015**, *5*, 1402321.
[40] L. Gil-Escrig, C. Momblona, M. Sessolo, H. J. Bolink, *J. Mater. Chem. A* **2016**, *4*, 3667.

7 Summary and outlook

In this work we have investigated various methods to prepare perovskite photovoltaic devices. The three goals set in the beginning of the research period had all been accomplished.

First, we have succeeded to establish a stable and reproducible method to fabricate solution processed perovskite solar cells, employing lead acetate and MAI as the precursor materials. The processing includes low temperature steps, compatible with solution-based deposition on plastic substrates, and thus it serves as a viable option for future production and upscaling. This feature arises from the volatility of methylammonium acetate, facilitating a rapid nucleation of the perovskite material already below 100 °C and leading to smooth films with complete substrate coverage. Another contribution is the replacement of the standard n-i-p architecture for a p-i-n one, allowing to use PCBM which can be processed at low temperature. The p-i-n layout also drastically reduces the electrical hysteresis, providing more reliability during J-V measurements. This route was established as a standard in our group and it was used to test new materials and as a reference to compare new methods.

We also managed to tune the band gap of mixed bromide – iodide perovskite materials to reach 2.0 eV, by taking advantage of the stabilizing properties of Cs and FA cations. We have investigated double-cation, double halide perovskite, $Cs_{0.15}FA_{0.85}Pb(Br_{0.7}I_{0.3})_3$ fabricated by an anti-solvent method. This absorber is optimized so that it can be complementary to MAPI in a double junction perovskite/perovskite solar cell. Though we were not able to completely eliminate the photo-instability present in mixed Br – I systems, as evidenced by PL measurements, the stabilization provided by the double cation system was enough to enable the fabrication of a solar cell with the highest reported efficiency at the time for an absorber with a band gap larger than 1.8 eV.

Finally, we have successfully implemented the $Cs_{0.15}FA_{0.85}Pb(Br_{0.7}I_{0.3})_3$ perovskite absorber into a perovskite/perovskite tandem solar cell structure with a high power output. Using a vacuum deposition method to fabricate doped electron and hole transport layers, we were able to create an efficient charge recombination layer that can be used in perovskite/perovskite tandem cells overcoming the difficulties of solution processing.

These results have contributed to the advance of the field of perovskite photovoltaics, and opened possible pathways for future commercialization. The subject of ongoing and future research is the investigation of alternative compositions that provide improved stability, moisture resistance, ease of processing, lead-free precursors, and the tunability to achieve tailored optical and electronic properties. Using advanced vacuum deposition methods, the co-evaporation of multi-component perovskites can be developed, and this would be a valuable tool to achieve high efficiency multi-junction perovskite/perovskite tandem solar cells.

8 Resumen en español

8.1 Introducción

8.1.1 El comienzo de las células solares de perovskita

Uno de los mayores problemas que la humanidad tiene que resolver en el siglo XXI es el de satisfacer las crecientes necesidades energéticas, y hacerlo de un modo sostenible. Aprovechar fuentes de energía renovables es el camino más obvio para conseguirlo. La energía solar es una de las alternativas más prometedoras, puesto que hay una enorme cantidad de potencia que llega a la tierra en forma de radiación electromagnética desde el sol. A pesar de ser intermitente y su distribución en la tierra desigual, es la fuente de energía renovable con mayor densidad de energía y, por lo tanto, la mejor candidata para reemplazar a las fuentes fósiles y nucleares. El mercado de la energía solar está en constante crecimiento, y se espera que los 235 GW de potencia generados en las instalaciones de todo el mundo en 2015 se multipliquen por dos en el año 2018.

Los dispositivos fotovoltaicos transforman directamente la energía solar en electricidad, eliminando pasos intermedios de conversión utilizados en la mayor parte de los modos habituales de producción de energía. Desde el desarrollo de la primera célula solar de silicio por los laboratorios Bell en 1954, con una eficiencia de conversión eléctrica del 6%, los módulos basados en este material han mejorados considerablemente sus prestaciones, llegando a dominar el mercado fotovoltaico. El precio de esta fuente de energía disminuye progresivamente y en muchos lugares ya ha alcanzado el mismo coste de producción que las fuentes de energías tradicionales. Aunque el silicio sea un material abundante y no tóxico, el proceso de purificación en forma cristalina es lento y consume una gran cantidad de energía. Asimismo, al ser un semiconductor con un ancho de banda indirecto, su coeficiente de

absorción es muy bajo, y se necesitan capas con espesores de varias micras para conseguir células solares de alta eficiencia. Estas limitaciones intrínsecas al silicio cristalino, impulsan el desarrollo de dispositivos fotovoltaicos más baratos y más eficientes, basados en materiales y modos de preparación alternativos. Las células solares de capa delgada – habitualmente denominadas células fotovoltaicas de segunda generación – utilizan materiales semiconductores que presentan una absorción de la luz varios órdenes de magnitud mayor al del silicio, permitiendo así la fabricación de dispositivos con capas activas mucho más delgadas. Al utilizar cantidades menores de semiconductor, es posible que sus costes de producción sean más reducidos. Las tecnologías más importantes son el telururo de cadmio (CdTe), el diseleniuro de indio, galio y cobre (CIGS), y el silicio amorfo hidrogenado (a-Si:H). Aunque estas tecnologías han demostrado su viabilidad comercial, su cota de mercado está por debajo del 10%.

Las células solares de tercera generación se basan en tecnologías fotovoltaicas emergentes de capa delgada, basadas en materiales avanzados con propiedades mejoradas. Entre estas propiedades cabe destacar la posibilidad de procesar las capas de semiconductores desde disolución, o de utilizar multicapas con absorción complementaria para superar el límite de eficiencia teórico de las células de una sola unión. Unos dispositivos prometedores han sido las células solares de colorante (DSSC), desarrolladas inicialmente por los investigadores del EPFL. El prototipo de esas células utiliza óxido de titanio (TiO_2) mesoporoso funcionalizado en la superficie con moléculas de colorantes capaces de absorber luz y transferir electrones al TiO_2. Las células DSSC tienen dos desventajas importantes, i) las moléculas de colorante contienen metales raros, como el rutenio, haciéndolas menos viables comercialmente, ii) utilizan electrolitos líquidos, perjudiciales para la estabilidad de la célula solar. Estos inconvenientes se han paliado parcialmente mediante el desarrollo de colorantes libres de metales y electrolitos de estado sólido. Sin embargo, las células DSSC se han abandonado

recientemente en favor de dispositivos más eficientes basados en perovskitas híbridas (orgánicas-inorgánicas) de haluro de plomo , debido a las excelentes propiedades de este grupo de materiales descritas en la siguiente sección.

8.1.2 Generalidades de las perovskitas: Estructura y propiedades

La estructura tridimensional genérica de las perovskitas hibridas es ABX_3, donde A y B son cationes mono y divalentes, respectivamente, y X es un anión. Los cationes de posición A son habitualmente escogidos entre metilamonio (MA), formamidinio (FA) o cesio (Cs^+), aunque también se ha demostrado el uso de otros cationes como el rubidio (Rb^+) o el guanidinio. Los cationes de posición B más comunes son el plomo (Pb^{2+}) y el estaño, mientras que los aniones más utilizados en aplicaciones fotovoltaicas son el yoduro (I^-) y el bromuro (Br^-). La fórmula ABX_3 fue descrita en primer lugar por Goldschmidt, quien definió el factor de tolerancia de la perovskita, una cantidad adimensional que describe la estabilidad de la red cristalina basándose en el tamaño de los iones que la constituyen. En general, puede predecirse una estructura tridimensional estable de perovskita si el factor de tolerancia está entre 0.8 y 1.0. El factor de tolerancia es una herramienta importante, puesto que puede predecir si una composición de ciertos iones será compatible con una estructura de perovskita y, por lo tanto, guiar la investigación sobre nuevos materiales para dispositivos opto electrónicos de alta eficiencia.

Los parámetros de red de la estructura cristalina dependen del radio iónico efectivo de los halogenuros, lo cual, junto con el metal divalente que se utilice, determina el ancho de banda del semiconductor. Esto se resolvió en 1978 por Weber, quien obtuvo perovskitas de halogenuros de plomo y metilamonio de diferentes colores, desde incoloro hasta el negro, variando la composición de halogenuro. Esto significa que el espectro de absorción puede variarse simplemente cambiando el halogenuro, llegando a cubrir la totalidad del espectro visible. Esta versatilidad es una característica única de las perovskitas , y se ha investigado en

numerosos trabajos demostrado la posibilidad de sintonizar el ancho de banda de las capas foto-activas en las células solares de perovskita.

Desde la primera observación de fotocorriente en el titanato de bario ($BaTiO_3$) en 1956, los investigadores han intentado fabricar células solares basadas en perovskitas de óxidos inorgánicos, pero su eficiencia de conversión de energía (PCE) no ha llegado a superar el 1%. En 1995 Mitzi y sus colaboradores demostraron una síntesis simple y a baja temperatura de la perovskita híbrida $MASnI_3$, e investigaron sus propiedades como material activo para transistores a efecto de campo. Fue en 2009 cuando Miyasaka y sus colaboradores utilizaron nanocristales de $MAPbBr_3$ (MAPBr) y $MAPbI_3$ (MAPI) como colorantes en células DSSC. Observaron que las células solares basadas en MAPI mostraban respuesta espectral hasta los 800 nm, y obtuvieron una PCE de 3.8%. Los dispositivos preparados en este trabajo inicial empleaban los mismos electrolitos líquidos tradicionalmente utilizados en células DSSC, y por tanto sufrían una rápida degradación de la perovskita (que es soluble en disolventes polares). Un logro importante llegó pocos años más tarde cuando los electrolitos líquidos se reemplazaron por semiconductores orgánicos de estado sólido. En 2012, dos publicaciones demostraron un aumento relevante en la eficiencia fotovoltaica utilizando spiro-OMeTAD como material de transporte de huecos. Kim y colaboradores desarrollaron un dispositivo mesoscópico de estado sólido basado en nanopartículas de MAPI, alcanzando una eficiencia del 9.7%. Lee y colaboradores prepararon una célula solar con una capa absorbente de MAPI policristalina, alcanzando una eficiencia del 10.9%. El hecho de que las células solares preparadas con esta nueva arquitectura tenían un mejor rendimiento comparado al obtenido con dispositivos de tipo DSSC, implicaba que la perovskita tenía un carácter ambipolar, con movilidades de electrones y huecos comparables.

Las perovskitas híbridas tienen una seria de propiedades que las hace un excelente candidato para aplicaciones fotovoltaicas. De Wolf y colaboradores investigaron el espectro de absorción

óptico de perovskitas MAPI y su relación con el rendimiento fotovoltaico. Utilizaron espectroscopia de desviación fototérmica (PDS) y espectroscopía de fotocorriente de transformada de Fourier, que permiten investigar la absorción óptica con alta resolución. Han observado que este tipo de material posee un coeficiente de absorción muy elevado, comparable a lo del GaAs, el material fotovoltaico con mejor rendimiento hasta la fecha. También midieron una energía de Urbach tan pequeña como 15 meV, lo cual indica un elevado orden en el material. Sus descubrimientos explican la pequeña diferencia entre el ancho de banda óptico de MAPI y el voltaje de circuito abierto (V_{oc}) de las células solares correspondientes, lo cual es una de las razones para el elevado rendimiento de estos dispositivos. Yin y sus colaboradores llevaron a cabo un estudio teórico sistemático para investigar las propiedades optoelectrónicas de los halogenuros de perovskita. Sus cálculos confirmaron un coeficiente de absorción óptico excepcionalmente alto, entre 10^4 y 10^5 cm^{-1} en la parte visible del espectro electromagnético, comparable al del arseniuro de galio. En los semiconductores tiene una importancia especial la naturaleza de las especies transportadoras de carga, por su implicación en el rendimiento foto-voltaico. Por esto hay varias publicaciones que investigan este aspecto de las perovskitas. Se ha demostrado que la energía de enlace excitónica está entre 19 y 45 meV, cercana a la energía térmica a temperatura ambiente (26 meV). Esta propiedad es especialmente relevante ya que implica que en dispositivos de perovskita los electrones y huecos fotogenerados existen como cargas libres. Manser y colaboradores investigaron la generación de transportadores de carga en capas de perovskitas utilizando espectroscopia de absorción transitoria en la escala de femtosegundos. El trabajo señala que hay una interconexión importante entre los excitones fotogenerados y los transportadores de carga libres, y en particular que la generación de estos últimos limita la formación de excitones. Estos resultados indican que la existencia de interfaces dador-aceptor no es un requisito para el funcionamiento de células solares de perovskita, y el uso de estructuras planas es una aproximación viable para conseguir dispositivos de alto

rendimiento. En los años siguientes, se han desarrollado diversos métodos para la deposición de capas de perovskitas de alta calidad. Estos experimentos estaban encaminados a entender como afectaba a la química de diversos precursores una multitud de técnicas y condiciones de procesado, y como esto contribuye a las propiedades optoelectrónicas de las capas delgadas de perovskitas. El logro de un mejor control sobre estos parámetros permitió la preparación de dispositivos con características óptimas. En solo unos pocos años se llegó a conseguir células solares con eficiencias que compiten con las mejores células basadas en silicio - con un récord certificado actualmente en 22.1% - consolidando así a las fotovoltaica basada en perovskitas como una potencial alternativa para la producción a gran escala de energía renovable. A continuación revisaremos los metodos principales para la fabricación de células solares de perovskitas.

8.1.3 Métodos de deposición de películas delgadas

Existen dos métodos principales para depositar capas delgadas de perovskitas: desde disolución y en vacío, dependiendo del medio empleado para depositar los precursores en el sustrato. Además, pueden ser ulteriormente categorizados según el número de pasos de deposición utilizados para la formación de la perovskita, y en la mayoría de casos las capas se forman mediante un método de un paso o mediante dos pasos. El método más simple y más directo es mediante el procesado desde disolución en un paso. En este caso, los precursores (halogenuros del metal B y del catión A) se disuelven en un disolvente polar. Dimetilformamida (DMF) o dimetilsulfóxido (DMSO) son los disolventes más utilizados, aunque también se han investigado otras alternativas como el gamma-butirolactona (GBL) o N-metil-2-pirrolidona (NMP). Aunque la implementación de este método es fácil, conseguir una control de la morfología de la capa resultante requiere un extenso conocimiento del mecanismo de formación

de la perovskita. En un proceso de dos pasos se deposita primero el compuesto de plomo y posteriormente se forma la perovskita por reacción con la sal orgánica mediante "spin coating" o "dip coating". La ventaja de este método es que es más simple controlar la deposición de las componentes aisladas, y permite la formación de capas homogéneas y continuas. El mayor inconveniente de este método es que el espesor final de la perovskita está limitado a una pocos cientos de nanómetros, debido al límite de difusión del compuesto orgánico en el interior de la capa policristalina de halogenuro de plomo. Esto limita, intrínsecamente, la fotocorriente máxima que puede obtenerse y por tanto, la eficiencia máxima de la célula solar. Yang y colaboradores desarrollaron un método de procesado de disolución asistido por vapor (VASP), en el que la transformación se consigue mediante exposición del halogenuro de plomo a vapores de yoduro de metilamonio (MAI).

En los métodos basados completamente en vapor, se sitúan los precursores en dos crisoles separados en el interior de una cámara de vacío, y se calientan hasta la temperatura de sublimación. De este modo, los vapores reaccionan y condensan en la superficie del sustrato, formando una capa delgada de perovskita a baja temperatura. Se han desarrollado también métodos en dos pasos adaptados al procesado en vacío. Aunque los métodos de deposición en vacío son fiables, la mayoría de los trabajos publicados utilizan el procesado desde disolución debido a que el procesado y la instrumentación son mucho más sencillos.

8.1.4 Ingeniería de disolventes

Debido a que la nucleación y el crecimiento de las capas de perovskitas depende en gran medida de la interacción del disolvente con los precursores y con el sustrato, es importante elegir un disolvente adecuado y ajustar las condiciones de deposición. De tal modo, el ajuste de estos

parámetros resulta ser una parte fundamental en el campo del procesado de células solares de perovskitas. Al principio, se estudiaron mezclas de disolventes para mejorar la morfología de las capas. Sucesivamente, Jeón y sus colaboradores publicaron un método en el que empleaban una mezcla de GBL y DMSO para la disolución del precursor y se trataba la muestra con tolueno durante el procesado mediante "spinning". El tolueno es miscible tanto con GBL como con DMSO, sin embargo es un mal disolvente para los precursores de la perovskita. Tratando la capa aún húmeda con el anti-disolvente en el momento adecuado, el disolvente residual en la superficie puede eliminarse inmediatamente obteniendo una capa uniforme de perovskita. Este método se emplea ampliamente para depositar capas policristalinas que dan lugar a dispositivos con elevado rendimiento. Las células solares más eficientes hasta la actualidad se han fabricado con la estrategia anti-disolvente.

8.1.5 Composición de los precursores

Los trabajos iniciales utilizaron mezclas de MAI y PbI_2 con estequiometría 1:1, sin embargo se observó que la morfología de las capas de perovskita depositada era de mala calidad, y no permitía el recubrimiento completo del sustrato. Los agujeros presentes en esas capas disminuyen la resistencia de la célula solar correspondiente, dando lugar a un rendimiento irregular. Se realizaron estudios para resolver este problema mediante el uso de aditivos en el precursor, como el cloruro de metilamonio (MACl), 1,8-dioctano (DIO), o ácido yodhídrico (HI), y se observó una mejora en la morfología de las capas. Los trabajos de Kim y Lee demostraron que el uso de $PbCl_2$ como fuente de plomo daba como resultado una mejoría en el rendimiento del dispositivo, principalmente debido a la mayor homogeneidad morfológica de la capa foto-activa. Se denominó al material como "halogenuro mixto de perovskita" $MAPbI_2Cl$. Más tarde, Colella y sus colaboradores demostraron como esta síntesis no produce

una mezcla estequiométrica de cloruro y yoduro, ya que el cloro solo existe como elemento traza. Estos descubrimientos impulsaron a la investigación sobre el efecto de los precursores y sus proporciones en el rendimiento de las células de perovskita resultantes. El papel de los precursores y de los aniones fue investigado por Moore y colaboradores, quienes concluyeron que la cinética de la cristalización puede ser alterada escogiendo distintos precursores de plomo. Se demostró que se pueden formarse materiales volátiles que tienen un papel muy importante durante la cristalización, ya que al salir del sistema durante el tratamiento térmico forman capas de perovskita pura y homogénea. Estos descubrimientos ayudaron a explicar el papel de los iones cloruro entre los precursores y ofrecieron nuevas posibilidades para una mejor nucleación y crecimiento a bajas temperaturas mediante el uso de precursores alternativos, como el nitrato de bromo $PbNO_3$, o el acetato de plomo $Pb(OAc)_2$. Se ha observado que además de la composición de los precursores, la relación estequiométrica también tiene un gran impacto en la morfología de las capas de perovskitas depositadas y su rendimiento fotovoltaico. Yan y colaboradores han llevado a cabo un análisis exhaustivo de diferentes precursores variando la relación entre el halogenuro de plomo y el catión orgánico. El estudio ha revelado que las disoluciones de precursor de perovskita son similares a dispersiones coloidales, y la coordinación de los complejos está relacionada con la relación molar de los materiales en el precursor. Mientras que sus resultados sugieren que un exceso de cationes orgánicos respecto al plomo es beneficioso para el rendimiento del dispositivo, otros trabajos han mostrado que un exceso de yoduro de plomo ofrece un mayor PCE. La complejidad de estos parámetros es aún mayor al tener en cuenta el envejecimiento de los precursores. Tsai y colaboradores han demostrado que los procesos de nucleación y crecimiento ocurren ya en el propio precursor durante la agitación de la disolución, y tienen un gran impacto sobre el tamaño de grano de la capa de perovskita. Estos resultados ponen de manifiesto la multitud y complejidad de parámetros que afectan a la formación de las capas de perovskita y pone de evidencia la

necesidad de investigarlos más profundamente para poder tener un mayor control sobre la formación de capas delgadas de perovskita.

8.1.6 Arquitectura de los dispositivos

Desde su evolución a partir de células de DSSC, las primeras células solares de perovskita se han fabricado utilizando capas de TiO_2 mesoscópico para transportar los electrones desde el material foto-activo. Esta estructura es aún la más común en las células de perovskita, y por esto se denomina comúnmente como arquitectura estándar. Con el rápido desarrollo de las células de perovskita, se han realizado investigaciones sobre una amplia gama de capas de transporte selectivo de carga. Hay dos esquemas principales dependiendo de la polaridad del electrodo transparente (contacto frontal). Cuando la capa de transporte de electrones (ETL) se deposita en el contacto frontal, el dispositivo tiene una estructura n-i-p, mientras que si se invierte la polaridad (la extracción de huecos ocurre en la cara en contacto con el sustrato), la arquitectura se denomina p-i-n.

Debido a que la absorción de luz y la generación de cargas siguen un decaimiento exponencial en función de la distancia de la superficie, una de las cargas (electrón o hueco) debe viajar una distancia mayor antes de poder ser extraído de la capa fotoactiva. Esto tiene implicaciones obvias en el rendimiento del dispositivo, puesto que la longitud de difusión de los electrones y de los huecos es diferente. Un aspecto aún más importante de la arquitectura del dispositivo en las células solares procesadas desde disolución, son las interacciones físico-químicas entre el precursor y la capa adyacente. Una célula solar típica con arquitectura n-i-p utiliza TiO_2 como capa transportadora de electrones (ETL) y spiro-OMeTAD (2,2',7,7'-tetrakis-(N,N-di-parametoxifenilamina)9,9'-espirobifluoreno) como capa transportadora de huecos (HTL). A

pesar de que las mayores eficiencias publicadas se hayan conseguido con dispositivos n-i-p similares, existen algunas desventajas asociadas a esta arquitectura. Para conseguir capas de TiO_2 de alta calidad, es necesario un tratamiento térmico por encima de 400 ºC, lo cual es incompatible con sustratos flexibles plásticos, complicando la fabricación de células solares mediante la técnica "roll-to-roll". Otra desventaja es la frecuente presencia de histéresis en las curvas densidad de corriente-voltaje (J-V), lo que dificulta una evaluación precisa del rendimiento de los dispositivos. Otro aspecto a tener en cuenta es la baja estabilidad del spiro-OMeTAD, lo cual impide la producción a gran escala de células solares basadas en este material. Es muy importante superar estas desventajas mediante el desarrollo de materiales y métodos de deposición alternativos.

Las células solares con arquitectura p-i-n utilizan estructuras similares a las de células fotovoltaicas orgánicas, y por lo tanto los típicos materiales tipo p empleados, son diversos grados del poli(3,4-etilendioxitiofeno) con sufonato de poliestireno (PEDOT:PSS), mientras que las capas de ETL se basan en derivados de fulereno. Se ha demostrado la compatibilidad con la fabricación a gran escala mediante técnicas de fabricación "roll-to-roll" debido a su simplicidad y su baja temperatura de procesado. Sin embargo, las células solares basadas en estos materiales presentan un rendimiento ligeramente inferior en comparación con las de tipo n-i-p.

8.1.7 Ingeniería de "bandgap"

Una de las características claves que hace que las perovskitas tengan una gran versatilidad es la posibilidad de ajustar su absorción en un amplio rango del espectro visible. Los aniones bromuro tienen la capacidad de modificar el ancho de banda (bandgap, en inglés) y las

prestaciones de las células solares basadas en MAPI, tal como demostraron Noh y colaboradores. En su trabajo, utilizaron mezclas estequiométricas de MAI/PbI_2 y de MABR/$PbBr_2$ para ajustar el "bandgap" de las capas de perovskita. Mientras que han demostrado que una variación de "bandgap" modifica la absorción en las capas de perovskita y la eficiencia cuántica externa (EQE) de las células solares correspondientes, el comportamiento de las células solares muestra una desviación respecto al ideal, con un V_{oc} menor de lo esperado al aumentar el ancho de banda. Además se mostró que la incorporación de una pequeña cantidad de Br mejora la resistencia a la humedad de las células solares. Eperon y colaboradores investigaron un sistema con composición $FAPb(I_xBr_{1-x})_3$, variando la relación entre aniones halogenuro. Este estudio develó que la energía de "bandgap" óptico (E_g) de este sistema puede ajustarse entre 1.48 y 2.23 eV. Sin embargo, el sistema no es capaz de formar una fase pura cuando el contenido de Br está entre $0.5 < x < 0.7$. Continuando este trabajo inicial, se han llevado a cabo diversos estudios dirigidos a conseguir ajustar el "ancho de banda de las perovskitas con la incorporación de bromuro, pero la mayoría de publicaciones observaron un V_{oc} menor de lo esperado. Hoke y colaboradores investigaron en detalle este efecto y encontraron que los sistemas mixtos yoduro-bromuro experimentan una segregación de fases reversible al someterlos a iluminación. Esto se sustenta en la aparición de señales complementarias en el espectro de fluorescencia y en patrón de difracción de rayos X diferentes de los sistemas $MAPb(I_xBr_{1-x})_3$. Slotcavage y colaboradores han demostrado que la separación de fases depende de la intensidad de la iluminación, siendo el efecto directamente proporcional al flujo luminoso. Este efecto puede reducirse mediante la modificación química de la perovskita. En particular, utilizando un catión de posición A adecuado que genere un estrés en la red cristalina puede evitarse el efecto de separación de fases. Comparando los diferentes trabajos, Slotcavage y colaboradores han postulado que la presencia de histéresis en las curvas J-V proviene de la migración del halogenuro en la red cristalina. A parte de los esfuerzos para

fabricar absorbentes con ancho de banda mayor que el de la perovskita MAPI, también se han investigado perovskitas con un ancho de banda más estrecho, para mejorar la eficiencia de células solares de unión simple. El intercambio del catión metilamonio por formamidinio, implica un ligero desviación hacia el rojo en la absorción, dando lugar a mayores foto-corrientes. Las perovskitas basadas en estaño y en mezclas de estaño-plomo son también buenos candidatos para conseguir un efecto similar. Sin embargo, debido a la rápida oxidación del estaño, las células solares que incorporan tales materiales mostraron inicialmente una baja eficiencia. Investigaciones posteriores demostraron que la adición de SnF_2 evita la formación de iones Sn^{4+}, abriendo el camino hacia células solares con alto rendimiento empleando perovskitas basadas en estaño. En 2017, Zhao y colaboradores han demostrado que una perovskita mixta de estaño-plomo con ancho de banda de 1.25 eV, alcanza una eficiencia del 17.6% en un dispositivo de unión simple .

Mientras que los trabajos recientes en ingeniería de "bandgap" han demostrado conseguir mejoras importantes en el rendimiento de los dispositivos, aún existe mucho margen de mejora.

8.1.8 Células solares tándem

El récord de eficiencia de las tecnologías comerciales más importantes disponibles está mejorando a una velocidad cada vez menor, puesto que se acerca al máximo rendimiento que permite el límite Shockley–Queisser para células solares de unión sencilla. La mayor limitación aparece por las pérdidas espectrales, puesto que la mayor parte de la energía no puede ser aprovechada por un único semiconductor debido a pérdidas por la no-absorción y termalización. El impacto de esta limitación puede ser disminuido desarrollando arquitecturas tándem, combinando semiconductores con absorción en un rango complementario del espectro. El límite en la eficiencia para un dispositivo tándem de 2 componentes es del 42%, calculado por De Vos.

8.2 Objetivo de la tesis

El objetivo de esta tesis fue el desarrollo de nuevos materiales y dispositivos con arquitecturas novedosas para hacer frente a diferentes retos tecnológicos:

I. Desarrollar un método que permita la preparación simple y reproducible de células solares de perovskita eficientes mediante procesado desde disolución. Esto es de gran relevancia para el futuro desarrollo de la fotovoltaica basada en perovskitas.

II. Estudiar varios métodos para sintonizar el "bandgap" de las perovskitas y preparar células solares capaces de dar un fotovoltaje elevado. Esto permitiría preparar células tándem, con absorción complementaria, potencialmente aumentando el máximo de eficiencia que puede lograrse mediante el empleo de perovskitas como capas fotoactivas.

III. El objetivo final es conseguir una célula solar tándem utilizando semiconductores orgánicos como capas transportadoras de carga y absorbentes de perovskita complementarios. Esto es un reto para el procesado desde disolución, puesto que debe cumplirse la ortogonalidad de los disolventes. Por tanto, para conseguir este objetivo, deberán utilizarse tanto métodos basados en disolución como en vacío.

8.3 Células solares de perovskita basadas en acetato de plomo

Entre 2012 y 2014 el número de publicaciones sobre células solares de perovskita creció rápidamente, y la eficiencia de los dispositivos aumentaba continuamente. La mayor parte de esos hallazgos era principalmente empírica, puesto que la química fundamental de los precursores de perovskita aún no se conocía bien, y con frecuencia era difícil reproducir los protocolos publicados. Una de las mayores dificultades en los métodos de un solo paso era que los films habitualmente eran inhomogéneos y discontinuos. Esto significaba que la célula solar resultante tenía una baja resistencia en paralelo, y era necesario utilizar contactos gruesos para evitar fugas en el dispositivo. Se observó cómo en disoluciones de PbI_2/MAI con estequiometría 1:1 se formaban complejos intermedios, y esas especies favorecían la cristalización en forma de columnas que impedían un recubrimiento uniforme del sustrato. Buin y colaboradores llevaron a cabo cálculos teóricos (DFT) y encontraron que un entorno pobre en yodo conlleva un crecimiento preferencial de dominios de perovskita cristalina, bajando la densidad de trampas electrónicas. Correlacionaron esos resultados con un mejor rendimiento de los dispositivos fabricados a partir de precursores con $PbCl_2$, anticipando que el uso de precursores libres de halogenuro, como $Pb(SCN)_2$ o el acetato de plomo $Pb(OAc)_2$, serían alternativas viables para obtener perovskitas de alto rendimiento. Zhang y colaboradores desarrollaron un método simple y reproducible utilizando $Pb(OAc)_2$ como precursor. El acetato de metilamonio tiene un punto de ebullición bajo, y abandona el sistema rápidamente durante el tratamiento térmico de la capa. Esto desplaza la reacción hacia la formación de la fase de perovskita, dando lugar a una rápida nucleación y un buen recubrimiento del sustrato, con una baja rugosidad. Esto también permite emplear una baja temperatura para el tratamiento de la capa de perovskita, lo cual resulta atractivo para la producción a gran escala. El mayor rendimiento conseguido en ese trabajo fue del 15.2%, en una estructura n-i-p. Mientras que tanto la morfología, como el

PCE logrado fueron interesantes, no se aprovechó todo el potencial del procesado a baja temperatura, puesto que los films de perovskita se depositaban sobre una capa de TiO_2 que previamente se había calentado hasta los 500 ºC. También existía una histéresis importante en las curvas J-V. De ahí el gran interés de aprovechar esa metodología en una arquitectura tipo p-i-n, la cual permite un procesamiento a baja temperatura y presenta muy baja histéresis. Los experimentos fueron satisfactorios y se lograron las metas. Concretamente hemos preparado capas de perovskita uniformes y libres de defectos, así como fabricado células solares p-i-n con esas capas, las cuales han tenido un comportamiento reproducible y libre de histéresis. Los tratamientos térmicos empleados son compatibles con el procesado sobre sustratos plásticos, mostrando que esta metodología puede ser aplicada a la fabricación a gran escala mediante "roll-to-roll".

8.4 Células solares de perovskita con elevado "bandgap"

Desde que se demostró la posibilidad de sintonizar el "bandgap" de las perovskitas mediante un simple cambio del halogenuro, ha habido múltiples intentos de desarrollar estos materiales con propiedades de absorción de la luz específicas. Debido a que el "bandgap" de la perovskita MAPI es del orden de 1.55 eV, muy superior a 1.1 eV que es el valor óptimo requerido para conseguir la máxima eficiencia teórica en células de unión simple, una primera aproximación es disminuir el "bandgap" para conseguir la mayor corriente posible. Por otra parte, un "bandgap" de alrededor de 1.75 eV es compatible con una célula solar tándem de Si/perovskita. Algunos investigadores han descubierto que la incorporación de diversos iones tiene efectos en las propiedades ópticas, las posibilidades de procesado, y la estabilidad del material resultante. Los cationes de FA reducen el "bandgap" y aportan una mejor resistencia térmica, sin embargo, si el catión es más grande que MA, se requiere un tratamiento térmico a mayor temperatura

para superar la temperatura de activación y favorecer su inserción en la red cristalina. Otros cationes más pequeños implican un mayor "bandgap" y una resistencia térmica y a la humedad superiores. El intercambio de I por Br da lugar a un mayor "bandgap" así como una estabilidad del dispositivo mejorada. Sin embargo, tal como apuntan varios trabajos, la perovskita mixta $MAPb(I_{1-x}Br_x)_3$ no es estable bajo iluminación cuando el contenido en Br está entre 0.2 y 0.6. Con la introducción del método anti-disolvente, es relativamente fácil probar nuevas formulaciones con homogeneidad morfológica. De ahí que haya sido posible fabricar células solares eficientes y estables empleando capas de perovskita de diferentes propiedades ópticas de absorción. La mayor parte de estos trabajos se dirigieron a aumentar la absorción hacía la zona infrarroja del espectro solar, para conseguir células solares sencillas de mayor eficiencia, o al desarrollo de perovskitas con un elevado "bandgap" adecuado para formar parte de una célula tándem Si/perovskita. Por el contrario, ha habido pocos estudios dedicados al desarrollo de células tándem perovskita/perovskita, debido a las mencionadas dificultades en lo referente al procesado del dispositivo y la baja estabilidad de los sistemas mixtos I-Br. Nuestro trabajo ha estado dirigido a la creación de perovskitas de "bandgap" ancho, adecuadas para su uso en dispositivos tándem que utilizan MAPI como absorbente complementario. Hemos investigado una serie de perovskitas con composiciones $Cs_{0.15}FA_{0.85}Pb(Br_xI_{1-x})_3$ usando el método anti-disolvente y en arquitectura de dispositivo n-i-p. Hemos escogido optimizar $Cs_{0.15}FA_{0.85}Pb(Br_{0.7}I_{0.3})_3$ debido a su "bandgap" óptico de 2.0 eV, que es próximo al óptimo para su aplicación en células tándem con una sub-celda de "bandgap" 1.55 eV (MAPI). Hemos empleado una técnica de preparación mixta, realizando una parte desde disolución y otra parte mediante deposición en vacío, y hemos sido capaces de fabricar células solares eficientes con las propiedades de absorción deseadas. Incluso, aunque nuestros estudios de fotoluminiscencia han mostrado que la foto-inestabilidad no se elimina completamente, aun en presencia de cationes de Cs y FA, hemos sido capaces de fabricar los dispositivos fotovoltaicos basados en

perovskita con un "bandgap" mayor de 1.8 eV más eficientes hasta la actualidad. Es particularmente importante el haber conseguido un mayor V_{oc} (mayor que los dispositivos MAPI) y un factor de llenado (FF) muy alto, lo cual indica que esta estructura de perovskita permitiría una ganancia neta en eficiencia respecto a los dispositivos de unión simple, al incorporarla en una arquitectura tándem.

8.5 Células tándem perovskita-perovskita

Tal como se ha descrito en capítulos anteriores, el desarrollo de dispositivos tándem de perovskita/perovskita conlleva diversos retos tecnológicos significativos. Junto a las dificultades que aparecen por el procesado de arquitecturas multicapa desde disolución, un reto adicional que debe superarse en un tándem monolítico es la preparación de capas eficientes para la recombinación de cargas (CRL) entre los materiales activos. Las CRL deben poseer una alta conductividad y transparencia, para evitar pérdidas durante la producción de la energía, y deben ser compatibles con el procesado de multicapas. Algunos sistemas conocidos para la preparación de capas CRL son semiconductores orgánicos ampliamente empleados en los dispositivos orgánicos emisores de luz (OLED) y en células solares orgánicas. Utilizando técnicas de deposición en vacío, el proceso es simplemente aditivo, puesto que la deposición es totalmente independiente del sustrato. Puesto que ya hemos demostrado la preparación de células solares de perovskita de gran eficiencia y alto "bandgap", nuestra siguiente meta fue su incorporación en una arquitectura tándem. En esta parte de la tesis, hemos creado una célula solar tándem multicapa con arquitectura n-i-p perovskita/perovskita, empleando semiconductores orgánicos intrínsecos y dopados. Sobre una capa de $Cs_{0.15}FA_{0.85}Pb(Br_{0.7}I_{0.3})_3$ depositamos un capa CRL, utilizando N4,N4,N4’’,N4’’-tetra([1,1’-difenil]-4-yl)-[1,1’,4’,1’’-terfenil]-4,4’’-diamino (TaTm) como HTL, fullereno C60 como capa ETL, y 2,2’-

(perfluoronaftaleno-2,6-diilideno)dimalononitrilo (F_6-TCNNQ) como dopante tipo p y N1,N4-bis(tri-p-tolilfosforonanilideno) benceno-1,4-diamina (PhIm) como el dopante tipo n, respectivamente.

La célula solar tándem de perovskita preparada mostró un V_{oc} próximo a la suma de los voltajes de cada una de las sub-celdas, indicando la eficiencia de las capas CRL. En esta estructura hemos logrado un máximo de eficiencia del 18.1%, muy próximo al de una célula MAPI simple. La principal limitación de este valor radica en la foto-inestabilidad del absorbente con ancho de banda más amplio, lo cual da lugar a una limitada contribución al voltaje. También este dispositivo tándem podría mejorarse aún más sintonizando el "bandgap" de ambos absorbentes a valores más óptimos. A pesar de estos inconvenientes, hemos demostrado una estrategia viable para fabricar células solares tándem de perovskita/perovskita, que pueden ser incluso utilizadas para dispositivos de unión triple con células de silicio o células CIGS.

8.6 Resumen y perspectivas

En este trabajo hemos estudiado diferentes métodos para preparar dispositivos fotovoltaicos de perovskitas. Se han cumplido los tres objetivos definidos al inicio de este periodo de investigación.

En primer lugar, hemos establecido con éxito un método estable y reproducible para la fabricación de células solares de perovskita procesadas desde disolución, empleando acetato de plomo y MAI como materiales precursores. El proceso incluye pasos a baja temperatura, compatible con la deposición sobre sustratos plásticos desde disolución, representando así una opción viable para su producción a gran escala. Esta característica surge de la volatilidad del acetato de metilamonio, que facilita la rápida nucleación de la perovskita por debajo de 100 ºC

dando lugar a capas uniformes y de baja rugosidad, con un recubrimiento completo del sustrato. Otra contribución es la sustitución de la arquitectura estándar n-i-p por una p-i-n, lo cual permite el uso de PCBM, que puede procesarse a baja temperatura. El esquema p-i-n también reduce drásticamente la histéresis eléctrica, proporcionando mayor fiabilidad durante las medidas J-V. Esta ruta se estableció como un estándar en nuestro grupo, y se utilizó para probar nuevos materiales y como referencia para comparar nuevos métodos.

También hemos conseguido sintonizar el "bandgap" de perovskitas mixtas de bromuro y yoduro para alcanzar un valor de 2.0 eV, aprovechando las propiedades estabilizadoras de los cationes Cs^+ y FA. Hemos investigado perovskitas de doble halogenuro y doble catión $Cs_{0.15}FA_{0.85}Pb(Br_{0.7}I_{0.3})_3$, fabricadas con el método anti-disolvente. Este absorbente está optimizado de modo que puede ser complementario al MAPI en una célula solar de doble unión perovskita/perovskita. Aunque no hemos sido capaces de eliminar completamente la foto-inestabilidad presente en los sistemas mixtos Br/I, tal como evidenciaron las medidas de luminiscencia, la estabilización proporcionada por el sistema de doble catión es suficiente para permitir la fabricación de una célula solar con la mayor eficiencia reportada hasta la fecha por un absorbente con un "bandgap" mayor de 1.8 eV.

Finalmente, hemos implementado con éxito la perovskita $Cs_{0.15}FA_{0.85}Pb(Br_{0.7}I_{0.3})_3$ en una estructura de célula solar tándem perovskita/perovskita, con una alta eficiencia. Utilizando un método de crecimiento en vacío para fabricar capas dopadas para el transporte de electrones y huecos, fuimos capaces de crear capas de recombinación de cargas eficientes que pueden ser utilizadas en células tándem perovskita/perovskita superando las dificultades del procesado desde disolución. Estos resultados han contribuido al avance en el campo de las perovskitas fotovoltaicas y abre posibles caminos para una futura comercialización. La temática de las investigaciones actuales y futuras es el estudio de composiciones alternativas que proporcionen una mejor estabilidad y resistencia a la humedad, faciliten el procesado, utilicen precursores

libres de plomo, y con propiedades ópticas y electrónicas a medida. Utilizando métodos avanzados de crecimiento en vacío, puede desarrollarse la co-evaporación de perovskitas multi-componente. Esta sería una herramienta valiosa para conseguir células solares tándem de múltiple unión perovskita/perovskita de alta eficiencia.

Other contributions of the author

[1] Pérez-del-Rey, D., **Forgács, D**., Hutter, E. M., Savenije, T. J., Nordlund, D., Schulz, P., Berry, J. J., Sessolo, M. and Bolink, H. J. (2016), *Strontium Insertion in Methylammonium Lead Iodide: Long Charge Carrier Lifetime and High Fill-Factor Solar Cells*. Adv. Mater., **28**: 9839–9845.

[2] Gil-Escrig, L., Momblona, C., **Forgács, D.,** Pla, S., Fernández-Lázaro, F., Sessolo, M., Sastre-Santos, Á., and Bolink, H.J. (2016) *Interface engineering in efficient vacuum deposited perovskite solar cells*, Organic Electronics, Volume **37**, 396-401.

[3] Chen, Y.-F., Tsai, Y.-T., Bassani, D. M., Clerc, R., **Forgács, D**., Bolink, H. J. and Snaith, H. J. (2016). *Evidence of band bending induced by hole trapping at MAPbI 3 perovskite/metal interface*. J. Mater. Chem. A, **131**, 6050.

Bibliography

1. Jäger-waldau, A. *PV Status Report 2016 October 2016*. (2016). doi:10.2790/749737

2. Chapin, D. M., Fuller, C. S. & Pearson, G. L. A new silicon p-n junction photocell for converting solar radiation into electrical power [3]. *J. Appl. Phys.* **25,** 676–677 (1954).

3. Kane, E. O. Energy band structure in p-type germanium and silicon. *J. Phys. Chem. Solids* **1,** 82–99 (1956).

4. Green, M. A. *et al.* Solar cell efficiency tables (version 50). *Prog. Photovoltaics Res. Appl.* **25,** 668–676 (2017).

5. Shockley, W. & Queisser, H. J. Detailed balance limit of efficiency of p-n junction solar cells. *J. Appl. Phys.* **32,** 510–519 (1961).

6. O'Regan, B. & Gratzel, M. A Low-Cost, High-Efficiency Solar-Cell Based on Dye-Sensitized Colloidal TiO_2 Films. *Nature* **353,** 737–740 (1991).

7. Gong, J., Liang, J. & Sumathy, K. Review on dye-sensitized solar cells (DSSCs): Fundamental concepts and novel materials. *Renew. Sustain. Energy Rev.* **16,** 5848–5860 (2012).

8. Saliba, M. *et al.* Incorporation of rubidium cations into perovskite solar cells improves photovoltaic performance. *Science (80-.).* **354,** (2016).

9. Marco, N. De *et al.* Guanidinium: A Route to Enhanced Carrier Lifetime and Open-Circuit Voltage in Hybrid Perovskite Solar Cells. *Nano Lett.* **16,** 1009–1016 (2016).

10. Goldschmidt, V. M. Die Gesetze der Krystallochemie. *Naturwissenschaften* **14,** 477–485 (1926).

11. Saparov, B. & Mitzi, D. B. Organic–Inorganic Perovskites: Structural Versatility for Functional Materials Design. *Chem. Rev.* **116,** 4558–4596 (2016).

12. Weber, D. CH3NH3PbX3, a Pb(II)-System with Cubic Perovskite Structure. *Zeitschrift für Naturforsch. B* **33b,** 1443–1445 (1978).

13. Unger, E. L. *et al.* Roadmap and roadblocks for the band gap tunability of metal halide perovskites. *J. Mater. Chem. A* **5,** 11401–11409 (2017).

14. Setter, N. & Cross, L. E. The role of B-site cation disorder in diffuse phase transition behavior of perovskite ferroelectrics. *J. Appl. Phys.* **51,** 4356–4360 (1980).

15. Wang, F., Grinberg, I. & Rappe, A. M. Band gap engineering strategy via polarization rotation in perovskite ferroelectrics. *Appl. Phys. Lett.* **104,** 15–19 (2014).

16. Cava, R. J. *et al.* Bulk superconductivity at 91 K in single-phase oxygen-deficient perovskite Ba2YCu3O9. *Phys. Rev. Lett.* **58,** 1676–1679 (1987).

17. Mitzi, D. B., Feild, C. a., Schlesinger, Z. & Laibowitz, R. B. Transport, Optical, and Magnetic Properties of the Conducting Halide Perovskite CH3NH3SnI3. *J. Solid State Chem.* **114,** 159–163 (1995).

18. Kojima, a, Teshima, K., Shirai, Y. & Miyasaka, T. Organo Metal Halide Perovskites as Visible-Light Sensitizer for Photovoltaic Cells. *Priv. Commun.* **1,** 1 (2009).

19. Kim, H.-S. *et al.* Lead Iodide Perovskite Sensitized All-Solid-State Submicron Thin Film Mesoscopic Solar Cell with Efficiency Exceeding 9%. *Sci. Rep.* **2,** 591 (2012).

20. Lee, M. M., Teuscher, J., Miyasaka, T., Murakami, T. N. & Snaith, H. J. Efficient Hybrid Solar Cells Based on Meso-superstructured Organometal Halide Perovskites. *Science (80-.).* **338,** 643–647 (2012).

21. Wolf, S. de *et al.* Organometallic Halide Perovskites: Sharp Optical Absorption Edge and. *J. Phys. Chem. C* **5,** 1035–139 (2014).

22. Yin, W. J., Shi, T. & Yan, Y. Unique properties of halide perovskites as possible origins of the superior solar cell performance. *Adv. Mater.* **26,** 4653–4658 (2014).

23. Sun, S. *et al.* The origin of high efficiency in low-temperature solution-processable bilayer organometal halide hybrid solar cells. *Energy Environ. Sci.* **7,** 399 (2014).

24. Tanaka, K. *et al.* Comparative Study in the Excitons in Lead- Halide based Perovskite-type Crystals CH3NH3PbBr3 CH3NH3PbI3. *Solid State Commun.* **127,** 619–623 (2003).

25. Lin, Q. *et al.* Electro-optics of perovskite solar cells. *Nat. Photonics* **9,** 106 (2014).

26. Manser, J. S. & Kamat, P. V. Band filling with free charge carriers in organometal halide perovskites. *Nat. Photonics* **8,** 737–743 (2014).

27. Yang, W. S. *et al.* Iodide management in formamidinium-lead-halide–based perovskite layers for efficient solar cells. *Science (80-.).* **356,** (2017).

28. Gao, P., Grätzel, M. & Nazeeruddin, M. K. Organohalide lead perovskites for photovoltaic applications. *Energy Environ. Sci.* **1,** 2448–2463 (2014).

29. Chen, Q. *et al.* Planar heterojunction perovskite solar cells via vapor-assisted solution process. *J. Am. Chem. Soc.* **136,** 622–625 (2014).

30. Malinkiewicz, O. *et al.* Perovskite solar cells employing organic charge-transport layers. *Nat. Photonics* **8,** 128–132 (2014).

31. Chen, C. *et al.* Effi cient and Uniform Planar-Type Perovskite Solar Cells by Simple Sequential Vacuum Deposition. 6647–6652 (2014). doi:10.1002/adma.201402461

32. Jeon, N. J. *et al.* Solvent engineering for high-performance inorganic-organic hybrid perovskite solar cells. *Nat. Mater.* **13,** 1–7 (2014).

33. Lee, J. W., Kim, H. S. & Park, N. G. Lewis Acid-Base Adduct Approach for High Efficiency Perovskite Solar Cells. *Acc. Chem. Res.* **49,** 311–319 (2016).

34. Saliba, M. *et al.* Cesium-containing triple cation perovskite solar cells: improved stability, reproducibility and high efficiency. *Energy Environ. Sci.* **9,** 1989–1997 (2016).

35. Zhao, Y. & Zhu, K. CH 3 NH 3 Cl-Assisted One-Step Solution Growth of CH 3 NH 3 PbI 3 : Structure, Charge-Carrier Dynamics, and Photovoltaic Properties of Perovskite Solar Cells. *J. Phys. Chem. C* **118,** 9412–9418 (2014).

36. Liang, P.-W. *et al.* Additive enhanced crystallization of solution-processed perovskite for highly efficient planar-heterojunction solar cells. *Adv. Mater.* **26,** 3748–54 (2014).

37. Colella, S. *et al.* MAPbI3-xClx mixed halide perovskite for hybrid solar cells : the role of chloride as dopant on the transport and structural properties. *Chem. Mater.* **25,** 4613 (2013).

38. Moore, D. T. *et al.* Crystallization Kinetics of Organic–Inorganic Trihalide Perovskites and the Role of the Lead Anion in Crystal Growth. *J. Am. Chem. Soc.* 150209140709004 (2015). doi:10.1021/ja512117e

39. Yan, K. *et al.* Hybrid Halide Perovskite Solar Cell Precursors: Colloidal Chemistry and Coordination Engineering behind Device Processing for High Efficiency. *J. Am. Chem. Soc.* **137,** 4460–4468 (2015).

40. Bi, D. *et al.* Efficient luminescent solar cells based on tailored mixed-cation perovskites. *Sci. Adv.* **2,** e1501170–e1501170 (2016).

41. Roldan-Carmona, C. *et al.* High efficiency methylammonium lead triiodide perovskite solar cells: the relevance of non-stoichiometric precursors. *Energy Environ. Sci.* **8,** 3550–3556 (2015).

42. Tsai, H. *et al.* Effect of Precursor Solution Aging on the Crystallinity and Photovoltaic Performance of Perovskite Solar Cells. *Adv. Energy Mater.* 1602159 (2017). doi:10.1002/aenm.201602159

43. Song, Z., Watthage, S. C., Phillips, A. B. & Heben, M. J. Pathways toward high-performance perovskite solar cells: review of recent advances in organo-metal halide perovskites for photovoltaic applications. *J. Photonics Energy* **6,** 22001 (2016).

44. Wu, N. *et al.* Identifying the Cause of Voltage and Fill Factor Losses in Perovskite Solar Cells by Using Luminescence Measurements. *Energy Technol.* (2017). doi:10.1002/ente.201700374

45. Noh, J. H., Im, S. H., Heo, J. H., Mandal, T. N. & Seok, S. Il. Chemical management for colorful, efficient, and stable inorganic-organic hybrid nanostructured solar cells. *Nano Lett.* **13,** 1764–1769 (2013).

46. Eperon, G. E. *et al.* Formamidinium lead trihalide: a broadly tunable perovskite for efficient planar heterojunction solar cells. *Energy Environ. Sci.* **7,** 982 (2014).

47. Hoke, E. T. *et al.* Reversible photo-induced trap formation in mixed-halide hybrid perovskites for photovoltaics. *Chem. Sci.* **6,** 613–617 (2015).

48. Slotcavage, D. J., Karunadasa, H. I. & McGehee, M. D. Light-Induced Phase Segregation in Halide-Perovskite Absorbers. *ACS Energy Lett.* **1,** 1199–1205 (2016).

49. Jaffe, A. *et al.* High-Pressure Single-Crystal Structures of 3D Lead-Halide Hybrid Perovskites and Pressure Effects on their Electronic and Optical Properties. *ACS Cent. Sci.* acscentsci.6b00055 (2016). doi:10.1021/acscentsci.6b00055

50. Stoumpos, C. C., Malliakas, C. D. & Kanatzidis, M. G. Semiconducting tin and lead iodide perovskites with organic cations: Phase transitions, high mobilities, and near-infrared photoluminescent properties. *Inorg. Chem.* **52,** 9019–9038 (2013).

51. Hao, F., Stoumpos, C. C., Cao, D. H., Chang, R. P. H. & Kanatzidis, M. G. Lead-free solid-state organic–inorganic halide perovskite solar cells. *Nat. Photonics* **8,** 489–494 (2014).

52. Lee, S. J. *et al.* Fabrication of Efficient Formamidinium Tin Iodide Perovskite Solar Cells through SnF2-Pyrazine Complex. *J. Am. Chem. Soc.* **138,** 3974–3977 (2016).

53. Zhao, D. *et al.* Low-bandgap mixed tin–lead iodide perovskite absorbers with long carrier lifetimes for all-perovskite tandem solar cells. *Nat. Energy* **2,** 17018 (2017).

54. Vos, a De. Detailed balance limit of the efficiency of tandem solar cells. *J. Phys. D. Appl. Phys.* **13,** 839–846 (1980).

55. Jiang, F. *et al.* A two-terminal perovskite/perovskite tandem solar cell. *J. Mater. Chem. a* **4,** 1208–1213 (2016).

56. Heo, J. H. & Im, S. H. $CH_3NH_3PbBr_3$-$CH_3NH_3PbI_3$ Perovskite-Perovskite Tandem Solar Cells with Exceeding 2.2 V Open Circuit Voltage. *Adv. Mater.* n/a-n/a (2015). doi:10.1002/adma.201501629

57. Eperon, G. E. *et al.* Perovskite-perovskite tandem photovoltaics with optimized band gaps. *Science (80-.).* **354,** 861–865 (2016).

58. Gil-Escrig, L., Momblona, C., Sessolo, M. & Bolink, H. J. Fullerene imposed high open-circuit voltage in efficient perovskite based solar cells. *J. Mater. Chem. A* (2016). doi:10.1039/C5TA10574A

59. Buin, A. *et al.* Materials processing routes to trap-free halide perovskites. *Nano Lett.* **14,** 6281–6 (2014).